NASA Contractor Report 3127

# Analytic Studies on Satellite Detection of Severe, Two-Cell Tornadoes

George F. Carrier, Paul Dergarabedian,
and Francis E. Fendell

CONTRACT NAS1-14578
APRIL 1979

NASA

NASA Contractor Report 3127

# Analytic Studies on Satellite Detection of Severe, Two-Cell Tornadoes

George F. Carrier, Paul Dergarabedian,
and Francis E. Fendell
*TRW Systems and Energy*
*Redondo Beach, California*

**Prepared for**
**Langley Research Center**
**under Contract NAS1-14578**

National Aeronautics
and Space Administration

**Scientific and Technical**
**Information Office**

1979

CONTENTS

## SUMMARY

In previous work the authors have emphasized, from funnel-cloud-length interpretation, that the exceptionally severe tornado is characterized by peak swirl speed relative to the axis of rotation on the order of 90 m/s, with 100 m/s being close to an upper bound. Further, they have emphasized that the thermohydrodynamic achievement of the pressure deficit (from ambient pressure) necessary to sustain such swirls requires that a particular structure exist. Specifically, a dry, compressionally heated, relatively slow downdraft of air with tropopause-level properties must lie within an annulus of rapidly swirling, originally low-level air ascending on a near-moist-adiabatic locus of thermodynamic states. This so-called two-cell structure is analogous to the eye/eye wall structure that marks evolution of a tropical storm to a hurricane, albeit for the tornado the horizontal spatial scales are vastly reduced. The two-cell structure furnishes an observable possibly accessible to a passively instrumented, geosynchronous meteorological satellite with resolution refined for mesoscale phenomena, for early detection of a severe tornado. Accordingly, the low-level turnaround region, in which the surface inflow layer separates to become a free ascending layer is examined quantitatively; this is the first step in establishing properties of the two-cell structure of the severe tornado. From previously established properties of the surface inflow layer under the high-speed portion of the potential-vortex portion of the tornado (just prior to separation), the turnaround flow is satisfactorily modeled as inviscid, such that turbulent diffusion is relatively unimportant. Preliminary results indicate that swirl "overshoot," i.e., swirl speeds in the turnaround region in excess of the maximum achieved in the potential vortex, is modest.

## INTRODUCTION

In previous work (ref. 1), the authors discussed indicators of the evolution of a rotating thunderstorm (also, referred to as a tornado cyclone and a mesocyclone) to a storm of even greater severity. The relatively long-lived rotating thunderstorm (ref. 2) is characterized by a horizontal scale of 10 km and a vertical scale of 10 km, and by organized swirl with radial profile of Rankine-vortex type; that is, relative to the axis of rotation, the time-averaged azimuthal component of velocity increases monotonically with (cylindrical) radial distance from the axis to a peak value, and then decreases monotonically with further distance from the axis of rotation. The rotating thunderstorm, which tends to translate to the right of the mean ambient wind, has peak swirl of roughly 20 m/s; it is a vortex of one-cell type: low-level inflow, central ascent and upper-level outflow. About one-quarter to one-half of these storms evolve to a stage of greater severity in which a central, compressionally heated nonrotating central downdraft is inserted, such that the swirling updraft is displaced from the axis of rotation. Such tornadogenesis bears some analogy to the insertion of a relatively dry eye within an almost moist-adiabatic eye wall, the evolution that marks the intensification of a tropical storm to a hurricane (or typhoon) (e.g., ref. 3); of course the temporal and horizontal scales are greatly reduced for the midlatitude local-severe-storm phenomenon, relative to the tropical-cyclone phenomenon. Still, in both cases, the result is that dry nonrotating air whose thermodynamic state is roughly that of the ambient tropopause may descend at modest rate through the depth of the troposphere, and the resulting increased low-altitude pressure deficit of the storm center from ambient may sustain an increased rate of swirling of up to about 110 m/s. In both cases, the evolution to so-called two-cell structure (nonrotating central descent within an annulus of rapidly swirling ascent)

may proceed rather rapidly relative to the time scale for intensification of the one-cell vortex. In both the tropical-storm and local-severe-storm cases, about one-third to one-half of the formidable one-cell vortices intensify to the potentially devastating two-cell vortices.

Briefly, the authors (refs. 1,4) proposed that a necessary and sufficient condition for the exceedingly dangerous, exceptional tornado is the existence of an "eye" within an "eye wall"* (Figs. 1,2). The significance of this proposal is that it suggested the first explicit dangerous-tornado-indicating observable possibly accessible to a passively instrumented, geosynchronous meteorological satellite with resolution refined to mesoscale-phenomena requirements. The instrumentation of such a proposed satellite cannot penetrate the cirrus deck of the thunderstorm anvil. The "hole" in the cirrus shield generated by the compressional heating of descent may furnish a possible unique characteristic of the exceptionally dangerous tornado. Of course, the descent in the "eye" may not persist through most of the troposphere, so the tornado may not achieve extreme intensity; existence of a nascent "eye" does not assure either development or persistence of an "eye" extending through the depth of the troposphere. Also, early detection of an existing tornado, as distinct from anticipation of its onset, is the most that can be gleaned from the observable. Still, since the exceptional tornado can persist for over an hour and can have path length of 200 km, and since one rotating

*The suggestion that a compressionally heated central downdraft extending the depth of the tropopause could serve as the mechanism by which a pressure deficit consistent with about 100 m/s peak swirl could be achieved thermohydrodynamically, was set forth around 1970 by three research groups, independently (refs. 5-9). (Cf. refs. 10-15.)

thunderstorm can spawn a sequence of several such tornadoes in succession (ref. 16), the observable is one that might be exploited with significant benefit by a meteorological satellite, as part of an early-warning system.

The more common tornado, characterized by peak swirl of 50 m/s and by duration of ten minutes and by path length of a few kilometers, is of one-cell type. Without an "eye", and with only moist-adiabatic ascent to produce a lightening of weight (such that a horizontal pressure differential is generated at low altitude to sustain swirling), the more common tornado is consistent with a pressure deficit on the order of one-hundredth of ground-level atmospheric pressure. Such a tornado is not detectable by means of the observable just discussed, the "hole" in a cirrus shield. However, perhaps 98% of the death and destruction wrought by twisters is caused by approximately 2% of the total number of tornadoes (ref. 17). Thus, it seems appropriate to concentrate on an observable that characterizes the exceptional tornado of two-cell type, and which is consistent with a pressure deficit on the order of one-tenth of ground-level atmospheric pressure. Indeed, it may be speculated that "eye" insertion tends to be of periodic nature, such that a so-called supercell (i.e., a multiple-tornado-spawning tornado cyclone) often undergoes several transitions from one-cell to two-cell structure during its lifespan, which may be on the order of six hours (refs. 1,18).

Observors in aircraft flying over the cirrus shield of some well-developed thunderstorms have noted "hole formation" associated with local pronounced descending air flow and re-evaporation of condensed water substance by compressional heating (refs. 19,20). On the time scale of one-quarter to one-half hour, severe tornadogenesis occurred within the thunderstorm observed, on several occasions. It is reiterated that a nascent "eye" by no means assures that a two-cell structure fills the troposphere, so it is to be expected that, on some occasions, one or more

moderate-intensity tornadoes follow cloud-top descent. Of course, one-cell tornadoes may arise without any such "cloud collapse."

Recently, returns from dual pulsed Doppler radars have been interpreted to infer that tornadogenesis in a mesocyclone entails evolution from one-cell to two-cell structure (ref. 18). In particular, tornado onset is suggested to be coincident with the occurrence of a dry weak-reflectivity downdraft, within a swirling updraft with high reflectivity. Thus, the thesis proposed in ref. 1 is given further support.* (See also refs. 19-22.)

Establishing the spatial resolution that would be required for satellite detection of the downdraft "eye" seems worthwhile, even if such resolution currently is orders-of-magnitude finer than the resolution of existing instrumentation. The width of the tornadic "eye wall" in the upper troposphere, for a severe two-cell tornado, is an output to be ultimately extracted from the model in the work reported below. Also, one would like to know what properties characterize the "eye" and "eye wall" in the upper troposphere, because sufficient thermal anomaly in the compressionally heated core, over ambient temperatures at the same altitude, may be detectable one day.

Of course, the most direct procedure would be to concentrate entirely on the thermohydrodynamics of the upper-tropospheric flow in a two-cell model of a tall narrow intense atmospheric vortex. However, the tornado

*Inferences from radar returns should be drawn with caution. For example, radar returns are received first at midtropospheric altitudes from rotating thunderstorms, and only later are returns received from low levels (ref. 2). The inference is drawn that swirling develops first in midtroposphere and only later develops at lower altitudes. But radar depends on reflection off condensed water substance for a return, and so absence of a return does not mean, necessarily, that no swirling exists at low altitudes when swirling is observed in midtroposphere. In fact, while density stratification of the atmosphere modifies the applicability of the classical Taylor-Proudman theorem (ref. 23), still one suspects swirl is not confined to midtropospheric levels only. Since the condensation level descends as rotation increases (witness the descent of the tornado funnel cloud (ref. 24)), because energy is transferred to dynamic motion at the expense of static enthalpy, delayed low-level returns are quite plausible. (Cf. ref. 25.)

must be examined as a total flow system, in order to obtain the proper fluxes of mass, momentum, and heat into and away from the upper-tropospheric flow. Thus, one must model the entire tornado; in fact, the logical procedure is to "process" the tornado "throughput" analytically in the same sequence as the tornado "processes" the "throughput" in the field. Hence, one must commence with the low-level swirling inflow, proceed to the near-central swirling updraft, and only then undertake the high-level swirling outflow.

The authors are grateful for helpful technical discussions with Robert Costen of NASA Langley Research Center, Hampton, Virginia; his encouragement throughout this work is appreciated. The computer programs were written by Phillip Feldman; the graphical presentations were prepared by Asenatha McCauley; and the editing and typing of the manuscript were carried out by Patricia DeCuir.

## SYMBOLS

| | |
|---|---|
| C | the peak value achieved by the dimensionless streamfunction $\psi$ in the separated surface inflow layer |
| F* | the distribution of the quantity $(r^*v^*)^2$ as a function of $\psi^*$, $m^4/s^2$ |
| F | $F^*/\Gamma^{*2}$ |
| G* | the distribution of the total head as a function of $\psi^*$, $m^2/s^2$ |
| G | $G^*/V^{*2}$ |
| g* | acceleration of gravity, $m/s^2$ |
| h* | height of the surface inflow layer, m; also, thickness of the separated inflow layer, m |
| h | $h^*/r_1^*$ |
| I | the peak value of $\psi$ in the surface inflow layer just prior to separation |
| m | $(1+\bar{x}_o'^2)^{1/2}$; also, the perturbational value of $\chi$ at small values of $\theta$ |
| N | number of points used to resolve the separated-inflow-layer structure |
| n* | distance normal to a streamline, m |
| P | $(p^* - p_1^*)/\rho_d^* V^{*2}$ |
| $\bar{P}$ | $d\bar{x}/d\bar{z}$ |
| p* | pressure, kPa |
| p | $p^*/(\frac{1}{2}\rho_d^* V^{*2})$ |
| Q | $q^*/V^*$ |

| | |
|---|---|
| $q^*$ | $(u^{*2} + w^{*2})^{1/2}$, m/s |
| $r^*$ | cylindrical radial distance from the axis of symmetry, m |
| $s^*$ | distance along a streamline, m |
| $u^*$ | cylindrical radial velocity component, m/s |
| $u$ | $u^*/V^*$ |
| $V^*$ | the peak swirl speed in the potential portion of a vortex, m/s |
| $V$ | $v^*/V^*$ (also written as v) |
| $v^*$ | azimuthal (or tangential) velocity component, i.e., swirl, m/s |
| $v$ | $v^*/V^*$ (also written as V) |
| $w^*$ | axial velocity component, m/s |
| $X$ | $1 - [1 - (\psi/C)]^{1/2}$ |
| $x$ | $\pi r^*/h^*$ |
| $\overline{x}$ | $r^*/r_1^*$ (also written as X) |
| $y$ | $z^*/h^*$ |
| $z^*$ | axial coordinate, in cylindrical polar coordinates, m |
| $\overline{z}$ | $z^*/r_1^*$ |
| $\alpha$ | h |
| $\beta$ | h |
| $\Gamma^*$ | $r_1^* V^*$, $m^2/s$ |

$\Delta$ incremental distance in X

$\zeta$ $z^*/r_1^*$

$\theta$ angle giving the orientation of a streamline to a line parallel to the $z^* = 0$ plane; also, azimuthal coordinate

$\rho_d^*$ gas density, $kg/m^3$

$\phi$ $Q/(1 - X)$

$\chi$ $r^*/r_1^*$ (also written as $\overline{x}$)

$\psi^*$ streamfunction, $m^3/s$

$\psi$ $\psi^*/r_1^* \Gamma^*$

Subscripts:

a ambient ground-level value

i time node in a finite-difference grid

j spatial node in a finite-difference grid

o starting value; also, pertaining to the outer edge of the vortex

1 pertaining to the condition at which $v^* = V^*$

Superscripts:

$\sim$ perturbational quantity, dependent on X only

- dimensionless quantity (also denoted by absence of an asterisk)

* dimensional quantity

$\rightarrow$ vector quantity

$\hat{}$ unit vector

## ANTICIPATION OF TORNADOGENESIS

Before details of the "eye"/"eye wall" portion of a mature severe tornado are sought by modeling, some further brief comments on the use of geosynchronous mesoscale-resolution meteorological satellites for anticipation of tornadogenesis are set forth.

Typically, a midtropospheric minimum in the total static energy (the sum of static, gravitational, and potential-latent-heat-of-phase-change contributions), such that large low-level values are recovered in the upper troposphere only, is suggestive of local-severe-storm conditions in the midlatitudes. In fair weather, the profile of the total static energy increases monotonically with altitude in the midlatitudes. In moderately cloud-free areas, the mesoscale satellite seems incomparably capable of detecting convectively unstable situations by continuously measuring through the depth of the troposphere over broad expanses, by rapidly processing the sounding data, and by judiciously concentrating on suspect areas. The difficulty is that whether, when, and in what form the possible severe weather is to be manifested, today largely eludes understanding. Some appreciation of the role of vertical wind shear and internal gravity waves as severe-weather initiators has been attained, but tornado forecasting remains a remote goal. At present, modelers have not evolved stability analyses which indicate successfully the conditions under which a one-cell structure of a tornado cyclone becomes unstable to small disturbances, and might undergo a transition to a two-cell structure.

Thus, after but brief survey, one tends to doubt the near-term prospects of a mesoscale-resolution satellite as a means of anticipating tornado onset, and to concentrate on rapid detection of severe tornadoes.

## TORNADO MODELING: METHODOLOGY, AND A PROPOSED STRUCTURE

The modeling undertaken here is not an attempt to simulate the entire vortex system from the fundamental conservation laws and boundary conditions; others (refs. 26-28) are pursuing this course and we think that a contribution aimed at the understanding of the phenomena in particular regions within the storm would be of greater value than yet another overall study.

The methodology for modeling adopted here involves a conceptual subdivision of the mature severe vortex into logical parts, in each of which different physical phenomena dominate. Only the locally significant mechanisms are retained in treating each subdivision, and thus approximate methods of higher analysis (supplemented by modest computational effort) succeed in displaying parametric dependence explicitly and yielding physical insight. A composite solution might then be synthesized from the locally valid solutions by requiring appropriate continuity of dependent variables and fluxes at interfaces between subdomains. Here the four-part subdivision first introduced by Dergarabedian and Fendell (ref. 8), to model a mature, exceptionally severe tornado in time average as an axisymmetric vertical closed two-cell system extending from ground to tropopause, is adopted; there is diffusive flux, but no convective flux, of any quantity across any boundary. It is important to note that the incorporation of an "eye" is the major innovation of ref. 8 on earlier three-part structure proposed by Turner (ref. 29) and Barcilon (ref. 30).

The subdivisions are (Fig. 2): (I) a potential vortex and throughput supply, characterized by cyclostrophic and hydrostatic balances, with negligible radial influx; (II) a parabolic surface inflow layer, fed by very slow sinking from aloft and serving as a source of low-level swirling influx because of frictional forces ("teacup effect"); (III) a turnaround, "eye wall", and outflow region, in which air rises on a moist adiabat, the air ascending quickly enough to transport the condensed water substance

upward; and (IV) a nonrotating, slowly recirculating "eye" of dry air. The tornado is a once-through system, in which warm moist air in I descends slowly into II, the one region of the vortex in which friction dissipates angular momentum; the swirling influx in II is turned into a swirling upflow in III, the "eye wall" sloping away from the axis with height under conservation of angular momentum in a variable-density fluid; a larger pressure deficit from ambient (achieved by dry-adiabatic recompression in (IV)) is available to sustain large swirling speeds in I, owing to the outward slant of the "eye wall." The moisture-exhausted air that has been "processed" through the updraft annulus is deposited in the upper-tropospheric portion of region III, and does not interact with the "unprocessed" air remaining in region I. The "processed" air deposited in the upper portion of III is too dry to descend, then recirculate upward on a moist adiabat capable of sustaining a horizontal pressure deficit; tornado lifespans are too brief, anyway: if the air in the upper portions of III descended too quickly, compressional heating would destroy the radial pressure gradient between edge and axis requisite to sustaining high swirl (and the system would disintegrate). Suggestions by Deissler (ref. 31) that recirculation may occur seem unlikely. Exhaustion of the throughput of I, the lower total-static-enthalpy property of originally midtropospheric air of I, topographic disturbances, etc., cause eventual decay of the system. However, explanations for decay based on simple radial diffusion of angular momentum in time are incomplete and unsatisfactory.

It is now widely accepted that turbulent shear flow is <u>not</u> just a random "mess"; rather, spatially refined, time-dependent measurements reveal that these flows consist of coherent vortical interactive structures, such that the mean and instantaneous properties of the flow field may be quite divergent (ref. 32). The observation that a tall thin atmospheric vortex may contain transient smaller-scale vortices (so-called satellite or suction vortices) is about a century old (ref. 33). That unimodal distributions may not describe the character of fluctuations from the mean at

low altitudes in a tornado may evoke academic curiosity; but emphasis (refs. 19,34) on transient departures from axisymmetry appears premature in terms of the current status of whirlwind modeling, and seems digressive in terms of engineering-oriented concern with tornadoes (such as meteorological satellite requirements, nuclear power plant design, etc.).

## THE LOW-LEVEL INFLOW LAYER

The principal subject of the current study is the turnaround, updraft, and outflow subdivision of the tornado, region III. This subdivision has received relatively little attention, but examination of it is required to characterize the "eye" radius as a function of altitude.

Before attention can focus on region III, it is necessary to review what is known about the near-surface layer containing swirling inflow. The flow state at the exit of region II furnishes the flow state at the entrance of region III. The published solutions for the nonlinear parabolic boundary-value problem describing flow over a stationary surface under an intense vortex are far too many to enumerate, but only recently has lucid appreciation of the subtleties of the flow been achieved.

The outer flow in region I is a potential vortex: during spin-up, under convectively induced advection, fluid particles move closer to the axis about which they possess angular momentum. As soon as the pressure reduction by inflow and spin-up balances the pressure reduction achieved by near-moist-adiabatic ascent in the core, no further inflow is possible, and a quasi-steady state is achieved. Thus, in our model of the mature vortex, the outer boundary condition is approximately a potential vortex with negligible radial influx (ref. 8). At least as early as 1969 (refs. 35,36), results pertaining to a tornado boundary layer were reported in which, under a potential vortex without radial flow, the tangential velocity component monotonically decreases to zero from the inviscid-flow peak, as the ground is approached at fixed radial station. The radial inflow increases monotonically from zero in the

potential vortex to a near-ground peak, and then decreases rapidly to zero. Perhaps because the calculation is not carried in close enough to the axis of symmetry, the peak for the radial inflow at any fixed radial position never achieves values above about one-half the local swirl speed in the inviscid flow. In any case, these results furnish limited insight into boundary-layer structure; that contribution is made largely by analytic work now described (Figs. 3-6).

Carrier (ref. 37) and Burggraf, Stewartson, and Belcher (ref. 38) noted that, under an inviscid outer flow with swirl speed increasing with decreasing radial distance from the axis of rotation, the role of friction is confined to an ever-thinning sublayer of the near-ground inflow layer. This frictionally controlled sublayer is immediately contiguous to the ground and, under the inner high-speed portion of the vortex, is exceedingly thin; across this thin near-ground sublayer, the swirl is uniformly negligible, and the radial influx decreases from its local peak value (achieved at the outer edge of the thin sublayer, and virtually equal to the swirl speed of the inviscid outer vortex at the fixed radial position of interest) to zero (achieved at the ground) under the action of viscous effects. The preponderance of the surface inflow layer, which increases in thickness very modestly with decreasing distance from the axis of symmetry in the high-swirl portion of the vortex, is mostly inviscidly controlled. More specifically, at any height above the very thin near-surface sublayer, the conservation of radial momentum is a balance of pressure, centrifugal and inertial effects such that, at fixed radial position, the sum of the squares of the radial velocity component and of the azimuthal velocity component (the swirl) is approximately equal to the square of the local swirl of the outer potential vortex. The conservation of angular momentum is a balance of inertial and transverse-friction effects, but under the high-speed portions of the vortex, the role of friction on the continuing evolution of the swirl profile is not large. The conservation of axial momentum gives axial invariance of the pressure across the entire inflow layer in the conventional manner, and continuity reveals that a very small downward

drift feeds the radial influx (appreciable because the area over which the downward drift occurs is large). Of course, under the outer, slower portions of the potential vortex, i.e., further from the axis of rotation, the inflow layer is thinner, and friction is appreciable across the entire layer; however, it is the inner, higher-speed portions of the vortex that are relevant to the present objective of establishing the nature of the low-level inflow entering subdivision III. The point is that angular momentum is conserved along all streamlines with finite swirl emerging from region II and entering region III, because the flow across the width of the surface inflow layer (aside from the near-ground thin frictional sublayer), to excellent approximation, is inviscid. under the high-speed portion of the outer vortex (only). However, because of the role of friction during radial influx toward the tornado core in the outer portions of the surface layer II, the angular momentum of each emerging streamline differs. The angular momentum monotonically decreases from the peak value of the inviscid flow of region I for the outermost inflow-layer streamline, to zero for the streamline at the edge of the thin viscous near-wall sublayer. The extension of these results to a turbulent inflow layer is given by Carrier and Fendell (ref. 39), and, recently, a numerical study by Prahlad and Head (ref. 40) displays similar results.

An important implication of the results just discussed is that, for radial positions within the distance at which the potential-vortex model holds for the inviscid outer flow, one cannot prescribe the radial profile of the swirl. That swirl profile, together with the radial and the axial flow components, emerge in the solution of the problem. This observation seems particularly pertinent to the two-cell-structure severe-mature-tornado case, in which the surface boundary layer separates prior to reaching the axis of rotation. Then, the inviscid character of the turnaround, in which conservation of angular momentum describes spin-up from a different datum for each streamline of the turnaround with significant swirl, may produce a radial profile of the azimuthal velocity component at fixed height that

is not easily anticipated. Thus, work (ref. 41-47) that prescribes some sort of rigid-body-like profile for the outer swirl at radial positions within the distance from the axis at which the potential-vortex-type flow holds, seems inadequate.

Because the nature of the low-level flow in region II is important to the development given below for region III, it is noteworthy that, in addition to the laboratory measurements of refs. 36, 46, and 47, there are field markings indicating a strong radial influx, without rotation, into some tornadoes at ground level. The evidence is a so-called deposition line sometimes left behind in mud, sand, wood debris, etc., after tornado passage (refs. 48-50); small objects lie inclined toward the line tracing the path of the bottom of the axis, on both sides of the path. The objects lie pointing toward the trace of the axis, but deflected to some extent in the direction of whirlwind translation. Of course, existence of markings depends upon the surface traversed, and markings are not always easily interpretable, even if they do exist. Further, solid objects falling through a tornado may retain motion imparted by higher-level flow, where swirl is appreciable. So markings left by fallen objects may not be representative of the very-lowest-level flow field.

## PRELIMINARY REMARKS ON THE TURNAROUND REGION

The difficulty in treating the "eye wall" annulus, region III, is that one has a free-streamsurface problem at both confining streamsurfaces, the streamsurface demarcating the "eye"/"eye wall" interface and the streamsurface demarcating the "eye wall"/inviscid-potential-flow interface. The location of each boundary must be ascertained in the course of solution of the boundary-value problem.

Here, the flow in the turnaround region is formulated first in cylindrical-polar coordinates, and, in that coordinate system it is an elliptical problem. Alternatively, a thin-layer approximation can be

adopted, in which case the problem is reduced to an ordinary differential equation by averaging some annular properties over the thickness; the result is an estimate of radial displacement of the annular centerline as a function of "eye wall" properties. Finally, the "eye wall" problem is rendered a tractable initial-value-type problem by reformulation in terms of streamfunction and orientation coordinates and by numerical integration after finite-differencing.

The most interesting aspect of the solution is the manner in which the erupting boundary-layer streamlines run in toward the axis of symmetry, and then move away from the axis, with increasing altitude. In fact, the solution tends to be periodic with altitude, such that successive inward and outward excursions of the "eye wall" annulus provide the formal solution of the formulation. However, it is highly probable that this configuration becomes unstable and that the description is valid only locally in the turnaround region.

## A BOUNDARY-VALUE PROBLEM FOR THE TURNAROUND

An inviscid incompressible steady axisymmetric model of the turnaround region in a severe tornado is adopted; the cylindrical polar coordinates have their origin at the ground on the axis of rotation (and of symmetry) (Fig. 7).

The conservation of angular momentum and of mass may be written in the form

$$(r^*v^*)^2 = \Gamma^{*2}F(\psi), \tag{1}$$

$$-r^*u^* = \frac{\Gamma^*h^*}{\pi}\frac{\partial\psi}{\partial z^*}, \tag{2}$$

$$r^*w^* = \frac{\Gamma^*h^*}{\pi}\frac{\partial\psi}{\partial r^*}, \tag{3}$$

where $v^*$, $u^*$, $w^*$ are circumferential, radial, and axial components of velocity, $\Gamma^* = r_1^*V^*$, and $r_1^*$ is the radius at which the pressure in the potential vortex is the same as the pressure in the stagnant core. Super asterisk denotes a dimensional quantity; no asterisk, a dimensionless quantity. The cylindrical radial coordinate is $r^*$; the axial coordinate, $z^*$; the maximum height of the surface inflow layer, $h^*$; the streamfunction for the secondary flow (involving velocity components $u^*$, $w^*$, only), $\psi^*$. The function $F(\psi)$ describes the distribution of angular momentum, which, of course, is conserved on each streamline.

Conservation of radial momentum is implied by ($\rho_d^*$ is fluid density)

$$u^*\frac{\partial u^*}{\partial r^*} + w^*\frac{\partial u^*}{\partial z^*} + \frac{\partial}{\partial r^*}\left(\frac{p^*}{\rho_d^*}\right) = \frac{\Gamma^{*2}F(\psi)}{r^{*3}}, \tag{4}$$

and Bernoulli's equation is

$$\frac{u^{*2} + w^{*2}}{2} + \frac{p^*}{\rho_d^*} + \frac{\Gamma^{*2}F(\psi)}{2r^{*2}} + g^*z^* = \frac{\Gamma^{*2}}{2r^*_1{}^2} + \frac{p_1^*}{\rho_d^*} . \tag{5}$$

The gravitational contribution is negligible within the region of interest here and the pressure across the inlet of the turnaround region is constant, so (5) becomes

$$\frac{u^{*2} + w^{*2}}{2} + \frac{p^*}{\rho_d^*} + \frac{\Gamma^{*2}F(\psi)}{2r^{*2}} = \frac{\Gamma^{*2}}{2r_1^{*2}} + \frac{p_1^*}{\rho_d^*} , \tag{6}$$

where $p_1^*$ is the pressure at $r_1^*$. Within the potential vortex and in the boundary layer beneath it,

$$p_a^* - p_1^* \doteq (\rho_d^*/2)V^{*2} = (\rho_d^*/2)(\Gamma^{*2}/r_1^{*2}), \tag{7}$$

where $p_a^*$ is the ground-level ambient pressure (given).

From a crude treatment of the turnaround, to be published elsewhere, $(h^*/r_1^*) \doteq 0.2$ for relevant $r_1^*, V^*$, where typical (given) values, for a severe tornado, are $r_1^* \doteq 160$ m, $V^* \doteq 100$ m/s. In any case, $h^*$ and $r_1^*$ are taken as known. Thus, in addition to its use in (2) and (3), $h^*$ is employed to nondimensionalize the independent variables:

$$x = \pi r^*/h^* \quad , \quad y = \pi z^*/h^* . \tag{8}$$

Subtraction of the radial derivative of (5) from (4) gives

$$x\left(\frac{1}{x}\psi_x\right)_x + \psi_{yy} + \frac{F'(\psi)}{2} = 0 , \tag{9}$$

where subscripts x and y denote partial differentiation. The swirl profile $F(\psi)$ is known from conditions holding at $x = x_1 = \pi r_1^*/h^* \equiv \pi/h$. It is known that the flow in region II is such that F is a monotonically increasing function of $\psi$, where $F(0) = 0$ and $F(I) = 1$, and where the datum $\psi(x_1,0) = 0$

is adopted, and from (2) and (8),

$$\psi(x_1,\pi) = \int_0^{\pi} u(x_1,\zeta)\, d\zeta \equiv I, \tag{10}$$

where $u = u^*/V^*$, and $v = v^*/V^*$. Clearly, for F linear in $\psi$, (9) becomes Helmholtz's equation, and for F quadratic in $\psi$, (9) remains linear. Such simple forms for $F(\psi)$ are not detailed replications of $(r^*v^*)/\Gamma^*$ in region II, but they are potentially useful approximations.

The pressure along the streamline that separates from $y = 0$ at $x = x_1$ remains at $p_1^*$, for the model of a nonrotating "eye" isobaric at altitudes at which gravity plays no role. Then, from (6), since $F(0) = 0$,

$$(\psi_x)^2 + (\psi_y)^2 = \left(\frac{x}{x_1}\right)^2 \quad \text{on } \psi = 0. \tag{11}$$

The pressure along the streamsurface $\psi = I$, which passes through the circle $x = x_1$, $y = \pi$, should be consistent with the pressure in the potential-vortex region; hence

$$p(x,y) = p_1 + \left[1 - \left(\frac{x_1}{x}\right)^2\right], \tag{12}$$

where

$$p = \frac{p^*}{\frac{1}{2}\rho_d^* V^{*2}}. \tag{13}$$

From (6), (12), and (13), since $F(I) = 1$,

$$\psi_x^2 + \psi_y^2 = 0 \quad \text{on } \psi = I. \tag{14}$$

This condition merely states that there is no contribution from the secondary-flow velocity components u*, w* to the pressure field, where region III interfaces with region I.

Equations (9), (11), and (14) constitute the boundary-value problem of interest, when supplemented by a relation for $F(\psi)$, obtained from previously executed analysis of region II. By (1), (2), (6), and the fact that $w(x_1,y) \doteq 0$, the relation for $F(\psi)$ gives implicitly an expression for $\psi(x_1,y)$, $0 \leq y \leq \pi$, with which to initiate the analysis (see below). Finally, it is anticipated that $\psi(x,y)$, as given by the boundary-value problem is periodic in y; this periodicity reflects the fact that the formulation must be revised after completion of about one cycle. More explicitly, it is anticipated that the locus of any streamline, say $\psi = I/2$, as y increases, decreases to a minimum value of x, then increases in x to recover its initial value $x = x_1$ and to achieve a peak value in x, before decreasing back to $x = x_1$ to begin another period. It is to be expected that the undulating flow so generated will be unstable somewhere along its trajectory, but our present job is to find that flow and the stability problem is deferred until that is done. Of particular interest are the amount by which v exceeds the value associated with $x = x_1$, $\psi = I$, and the values of x and $\psi$ at which the maximum occurs.

For explicitness, a <u>rough</u> characterization of the function $\psi(x_1,y)$, $0 \leq y \leq \pi$, is now presented. In the largely inviscid portion of region II, (6) may be rewritten as

$$u^2(x,y) + v^2(x,y) \doteq (x_1/x)^2 \ . \tag{15}$$

From (1), (2), and (15), one obtains

$$-u(x_1,y) = \frac{\partial\psi(x_1,y)}{\partial y} = \left\{1 - [v(x_1,y)]^2\right\} = [1 - F(\psi)]^{1/2}, \tag{16}$$

where $0 \leq F(\psi) \leq 1$ for $0 \leq \psi \leq I$. Thus, $\psi(x_1,y)$ is given by

$$y = \int_0^{\psi(x_1,y)} \frac{d\mu}{\{1 - [F(\mu)]\}^{1/2}} \tag{17}$$

where $\psi \to I$ as $y \to \pi$ (cf. (10)). For $F(\psi) = \psi/I$,

$$\psi = y\left(1 - \frac{y}{2\pi}\right), \quad I = \frac{\pi}{2} \Rightarrow v^2(x_1,y) = \frac{2y}{\pi}\left(1 - \frac{y}{2\pi}\right). \tag{18}$$

For $F(\psi) = (\psi/I)^2$,

$$\psi = 2^{1/2}\sin(y/2), \quad I = 2^{1/2} \Rightarrow v^2(x_1,y) = \sin^2(y/2) . \tag{19}$$

In fact,

$$v(x_1,y) \doteq 1 - \exp\left(-\frac{c}{\pi}y\right), \quad c \doteq 3 , \tag{20}$$

might be more realistic, but is far less tractable.

In summary, if

$$\Psi(x,y) = \frac{\psi(x,y)}{I} , \quad G'(\Psi) = \frac{F'(\psi)}{I} , \tag{21}$$

Then the boundary-value problem is, for $0 \leq \Psi \leq 1$,

$$x\left(\frac{1}{x}\Psi_x\right) + \Psi_{yy} + G'(\Psi) = 0 ; \tag{22}$$

$$\Psi_x^2 + \Psi_y^2 = \left(\frac{x}{Ix_1}\right)^2 \quad \text{on } \Psi = 0, \qquad \Psi_x^2 + \Psi_y^2 = 0 \quad \text{on } \Psi = 1; \tag{23a}$$

$$\Psi(x_1,y) \quad \text{given, with } \psi \text{ periodic in } y. \tag{23b}$$

One might consider interchanging the roles of the dependent variable $\psi$ and the independent variable x, and using perhaps some technique within the framework of the method of weighted residuals, to extract the desired information from (21) - (23). Because the authors consider numerical treatment of (21) - (23) worth pursuing, the formulation has been set forth in some detail. However, alternative procedures are used in this report to study (21) - (23).

## TREATMENT OF A SEPARATED LAYER WITHOUT STRUCTURE

A momentum balance in an axisymmetric separated boundary layer without structure is examined. The thin sheet (or "eye wall") is the demarcation between any "eye," isobaric at pressure $p_1^*$, and a potential vortex with radially dependent pressure given by (12). At $r^* = r_1^*$, $p^*$ in the sheet equals that in the "eye" (Fig. 8).

Henceforth in this section the symbol $r^*(z^*)$ denotes the outside surface of the "eye wall" without structure. At the point A, given by $[r^*(z^*), z^*]$, the principal radii of curvature are $\left\{1 + [r^{*\prime}(z^*)]^2\right\}^{3/2}/r^{*\prime\prime}(z^*)$, the radius of curvature in a plane containing the axis of symmetry and the streamline on which point A lies, and $r^*(z^*)\left\{1 + [r^{*\prime}(z^*)]^2\right\}^{1/2}$, the radius of curvature in a plane perpendicular to the streamline on which point A lies. Super prime denotes ordinary derivative with respect to the argument of the function. The velocity component in a plane containing the axis of symmetry is denoted $q^*$, while the velocity component (swirl) in a plane perpendicular to the axis of symmetry is denoted $v^*$. Thus, if $\hat{t}$ is a unit vector in the plane containing the axis, and $\hat{\theta}$ is perpendicular to $\hat{t}$ and refers to the azimuthal component in a cylindrical-polar-coordinate system, then

$$\vec{v}^* = q^*\hat{t} + v^*\hat{\theta}. \tag{24}$$

The force balance perpendicular to the thin sheet at $[r^*(z^*), z^*]$ equates the pressure gradient consistent with a potential vortex outside the sheet, to the component of acceleration perpendicular to the sheet. There are two contributions to the acceleration, each involving the square of a velocity component over an appropriate radius of curvature:

$$-\frac{\partial}{\partial h^*}\left(\frac{p^*}{\rho_d^*}\right) = \frac{q^{*2} r^{*''}}{[1 + (r^{*'})^2]^{3/2}} - \frac{v^{*2}}{r^*[1 + (r^{*'})^2]^{1/2}} \tag{25}$$

where $h^*$ represents a coordinate running across the sheet.

Variations in velocity occurring across the sheet are not resolved ($\Gamma^* \equiv r_1^* V^*$):

$$\int v^{*2} dh^* = \Gamma^{*2} \int \frac{dh^*}{[r^*(h^*)]^2} = r_1^{*2} V^{*2} \int \frac{dh^*}{[r^*(h^*)]^2} \equiv \frac{r_1^{*2} V^{*2} A^*}{r^{*2}} \Rightarrow$$

$$\frac{A^*}{r^{*2}} = \int \frac{dh^*}{[r^*(h^*)]^2} \; ; \tag{26}$$

$$\int q^{*2} dh^* = V^{*2} \int \left[\frac{q^*(h^*)}{V^*}\right]^2 dh^* \equiv V^{*2} B^* \Rightarrow$$

$$B^* = \int \left[\frac{q^*(h^*)}{V^*}\right]^2 dh^* \; . \tag{27}$$

The potential-vortex form of $v^*$ is used in the definition of $A^*$.

From these definitions and from (12), to an accuracy that serves current purposes,

$$\frac{V^{*2}}{2}\left(1 - \frac{r_1^{*2}}{r^{*2}}\right) = \frac{A^*V^{*2}r_1^{*2}}{r^{*3}\left[1 + (r^{*\prime})^2\right]^{1/2}} - \frac{B^*V^{*2}r^{*\prime\prime}}{\left[1 + (r^{*\prime})^2\right]^{3/2}} . \tag{28}$$

The following nondimensionalization is introduced:

$$\bar{x} = \frac{r^*}{r_1^*} , \quad \bar{z} = \frac{z^*}{r_1^*} , \quad \alpha = \frac{2A^*}{r_1^*} , \quad \beta = \frac{2B^*}{r_1^*} . \tag{29}$$

If $A^* = (h^*/2)$, $B^* = (h^*/2)$, seemingly reasonable values, then

$$\alpha \doteq \frac{h^*}{r_1^*} \equiv h , \qquad \beta \doteq \frac{h^*}{r_1^*} \equiv h . \tag{30}$$

Under (29), (28) becomes ($\alpha$,$\beta$ specified)

$$1 - \frac{1}{\bar{x}^2} = \frac{\alpha}{\bar{x}^3(1 + \bar{x}^{\prime 2})^{1/2}} - \frac{\beta\bar{x}^{\prime\prime}}{(1 + \bar{x}^{\prime 2})^{3/2}} \quad \Rightarrow$$

$$\bar{x}^{\prime\prime} = \frac{\alpha}{\beta}\frac{1 + \bar{x}^{\prime 2}}{\bar{x}^3} - \frac{1}{\beta}\left(\frac{\bar{x}^2 - 1}{\bar{x}^2}\right)(1 + \bar{x}^{\prime 2})^{3/2} . \tag{31}$$

In this translationally invariant equation, it is taken that $\bar{x}(\bar{z} = 0) = 1$. It is shown below that $\bar{x}$ is periodic in $\bar{z}$. Solution is sought for positive and negative z, where the boundary conditions are

$$\bar{x}(0) = 1 \tag{32}$$

$$\bar{x}'(0) = \bar{x}'_0, \text{ given const.} > 0. \tag{33}$$

The boundary conditions preclude odd or even solution for $\bar{x}$ in $\bar{z}$. Sought are $\bar{x}^+$, the largest value of $\bar{x}$, which occurs where $\bar{x}' = 0$, and $\bar{x}^-$, the smallest value of $\bar{x}$, which also occurs where $\bar{x}' = 0$. In that $\bar{x}^- < 1$, there is "overshoot" of the swirl, and, from (12), there is decrease of pressure from the value that holds in the "eye", i.e., in $0 < r^* < r^*(z^*)$; it is reiterated that the magnitude of the swirl overshoot and pressure decrease are of particular interest.

While numerical integration of (31) - (33) is required ultimately, some preliminary treatment is helpful. Since (31) is translationally invariant in $\bar{z}$, phase-plane analysis is introduced (Fig. 9):

$$\frac{d\bar{x}}{d\bar{z}} = \bar{P}(\bar{x}) \Rightarrow \frac{d^2\bar{x}}{d\bar{z}^2} = \frac{d\bar{P}(\bar{x})}{d\bar{z}} = \frac{d\bar{x}}{d\bar{z}}\frac{d\bar{P}}{d\bar{x}} = \bar{P}\frac{d\bar{P}}{d\bar{x}}. \tag{34}$$

Thus,

$$\frac{\beta\bar{P}\bar{P}'}{(1 + \bar{P}^2)^{3/2}} = \frac{\alpha}{\bar{x}^3(1 + \bar{P}^2)^{1/2}} + \frac{1}{\bar{x}^2} - 1. \tag{35}$$

The slope is infinite at $\bar{P} = 0$ and is zero where

$$\frac{\alpha}{\bar{x}^3(1 + \bar{P}^2)^{1/2}} + \frac{1}{\bar{x}^2} - 1 = 0 ; \tag{36}$$

the intersection of the curve of (36) with the $\bar{P} = 0$ ray is given by

$$\frac{\alpha}{\bar{x}_*^3} + \frac{1}{\bar{x}_*^2} - 1 = 0 \ , \tag{37}$$

where $\bar{x}_* = 1$ for $\alpha = 0$, $\bar{x}_* > 1$ for $\alpha > 0$. For $1 >> \alpha > 0$, $\bar{x}_* = 1 + (\alpha/2) - (3\alpha^2/8) + \ldots$

Although the following development is not pursued to the extent of obtaining results, it may be worth noting that if

$$H(\bar{x}) = (1 + \bar{P}^2)^{-1/2} \ , \tag{38}$$

then (35) becomes

$$-\beta H' = \frac{\alpha H}{\bar{x}^3} + \frac{1}{\bar{x}^2} - 1 \ . \tag{39}$$

If

$$\tau = \bar{x}^{-2} \ , \tag{40}$$

then

$$2\beta \frac{dH}{d\tau} - \alpha H = \tau^{-1/2} - \tau^{-3/2} \ , \tag{41}$$

or

$$H = (\beta\tau^{1/2})^{-1} - \left(\frac{\pi}{2\alpha\beta}\right)^{1/2} \left(1 + \frac{\alpha}{\beta}\right) \exp\left(\frac{\alpha\tau}{2\beta}\right) \operatorname{erfc}\left(\frac{\alpha\tau}{2\beta}\right)^{1/2}$$

$$+ E \exp\left(\frac{\alpha\tau}{2\beta}\right) \ , \tag{42}$$

where E is a const. of integration. From (38), (40), and the definition $\bar{P} \equiv (d\bar{x}/d\bar{z})$, one may write formally

$$\frac{d\bar{x}}{d\bar{z}} = \left\{1 + [H(\tau)]^{-2}\right\}^{1/2} = \frac{d(\tau^{-1/2})}{d\bar{z}} . \tag{43}$$

Thus,

$$d\bar{z} = \frac{d(\tau^{-1/2})}{\left\{1 + [H(\tau)]^{-2}\right\}^{1/2}} , \tag{44}$$

where $H(\tau)$ is given by (42).

For the special case $\alpha = 0$, i.e., no swirl, multiplication of (35) by $\bar{x}'$ yields

$$\frac{\beta}{(1 + \bar{x}'^2)^{1/2}} = \frac{(\bar{x} - 1)^2}{\bar{x}} + \frac{\beta}{m} , \tag{45}$$

where the constant of integration has been written as $(\beta/m)$, with

$$m \equiv (1 + \bar{x}_o'^2)^{1/2} \tag{46}$$

for consistency. It is recalled that $\bar{x}_o' (\equiv d\bar{x}(0)/d\bar{z})$ is a given positive finite constant. Inspection of (45) reveals that $\bar{x}'$ is maximum at $\bar{x} = 1$, so $(1 + \bar{x}_o'^2)^{1/2}$ is the maximum value of $(1 + \bar{x}'^2)^{1/2}$, whence the symbol m. At $\bar{x}' = 0$,

$$\bar{x}^{\pm} = 1 + \frac{\beta}{2}\left(1 - \frac{1}{m}\right) \pm \left[\frac{\beta}{2}\left(1 - \frac{1}{m}\right)\right]^{1/2} \left[2 + \frac{\beta}{2}\left(1 - \frac{1}{m}\right)\right]^{1/2} \tag{47}$$

For $\bar{x}_o' \to 0$ so $m \to 1$, $\bar{x}^{\pm}$ merge to unity; this case involves a vertically separating surface inflow layer, and hence no overshoot. For $\bar{x}_o' \to \infty$ so $m \to \infty$, $x^{\pm}$ remain bounded:

$$\bar{x}^{\pm} = 1 + \frac{\beta}{2} \pm \left(\frac{\beta}{2}\right)^{1/2} \left[2 + \frac{\beta}{2}\right]^{1/2} ; \qquad (48)$$

this case involves effectively horizontal inflow of the separating surface inflow layer, and leads to the minimum value of $\bar{x}^-$ for fixed $\beta$. For $\beta = 0.1$, $\bar{x}^+ \doteq 1.37$ and $\bar{x}^- \doteq 0.73$; for $\beta = 0.2$, $\bar{x}^+ \doteq 1.56$ and $\bar{x}^- \doteq 0.64$. The plausible range of $\beta = 0(0.2)$, from a crude analysis of the turnaround to be published separately; it is recalled that $\beta$ is associated with in-plane motion. These results suggest what proves to be a general trend: $\bar{x}^-$ decreases as $\bar{x}_0'$ and $\beta$ increase.

Finite values for $\alpha$ indicate finite swirl; increasing $\alpha$ yields larger $\bar{x}^-$ and smaller overshoot. From results of numerical integration, for finite $\alpha$, $\bar{x}^{\pm}$ approach finite values as $\bar{x}_0' \to \infty$ for fixed $\beta$. For the plausible values $\alpha = \beta = 0.2$, for $\bar{x}_0' = 2, 5, 10$, the corresponding values of $\bar{x}^- = 0.77$, 0.72, 0.70. Hence, swirl overshoots in the range of about 10% seem plausible, but no more; estimates that swirl in the turnaround exceeds the swirl at $\bar{x} = 1$, $\bar{z} = h$ (in terms of the definitions of (29)) by about 100% (ref. 26) are excessive according to this analysis. Further results are given in Table 1 and graphical presentation is given in Figures 10 and 11.

## A MARCHING-TYPE TREATMENT OF THE TURNAROUND WITH STRUCTURE

A model problem is adopted to study in more detail the local configuration within which transition occurs, from radial swirling boundary-layer inflow to vertical swirling "eye-wall" upflux, for a steady, largely inviscid vortex. Slightly idealized distributions for the radial and circumferential velocity components at a particular radius are adopted as input. The model problem requires that the streamline which is closest to the axis of symmetry, and which constitutes the "eye"/"eye wall" interface, is adjacent to a stagnation region of constant pressure, denoted $p_1^*$, and determined in a more complete model by hydrostatic considerations in the vertical; here, $p_1^*$ is taken as given. It is recalled that at radius $r_1^*$, at which the surface-boundary-layer

"inlet flow" to the turnaround is prescribed, the pressure associated with the outer vortical flow of region I is also $p_1^*$. Again, of particular interest is the largest amount by which the speed in the transition region exceeds that at $r^* = r_1^*$. It is reiterated that since the flow emerging from the boundary layer is largely inviscid, the analysis for the turnaround is also to be inviscid.

Conservation of mass and momentum are written in unconventional form because it is convenient to adopt as independent variables (coordinates) the streamfunction for the velocity in the $(r^*,z^*)$ plane, and the angle $\theta$ giving the orientation in that plane of the streamline relative to a line in the plane parallel to $z^* = 0$ (Fig. 12).

The streamfunction $\psi^*$ is defined by

$$r^*q^* = \frac{\partial\psi^*}{\partial n^*} , \tag{49}$$

where $r^*$ again denotes the conventional cylindrical radial coordinate at which the velocity is to be calculated, $q^*$ is the velocity in the $(r^*,z^*)$ plane, and $n^*$ is the distance normal to the streamline. The streamfunction of (49) is identical, of course, with the streamfunction for which (see (2) - (3))

$$r^*u^* = -\frac{\partial\psi^*}{\partial z^*} , \tag{50}$$

$$r^*w^* = \frac{\partial\psi^*}{\partial r^*} , \tag{51}$$

where $u^*$ and $w^*$ are the radial and axial velocity components, respectively, and $z^*$ is the axial coordinate.

The circumferential velocity $v^*$ obeys the angular-momentum-conservation requirements (see (1))

$$r^{*2}v^{*2} = F^*(\psi^*) , \tag{52}$$

with $F^*(\psi^*)$ determined when the velocity distribution of $v^*$ at $r^* = r_1^*$ is prescribed. The principal curvatures of a surface $\psi^* = \text{const.}$ are $(\partial\theta/\partial s^*)$ (in the $(r^*,z^*)$ plane, where $s^*$ is distance along the streamline) and $\sin\theta/r^*$.

The conservation of momentum along a streamline is equivalent, in the inviscid theory, to the statement that the total head is a function of $\psi^*$ only, i.e.,

$$\frac{q^{*2}}{2} + \frac{v^{*2}}{2} + \frac{p^*}{\rho_d^*} = \frac{G^*(\psi^*)}{2} + \frac{p_1^*}{\rho_d^*} \quad . \tag{53}$$

From comparison of (53) and (5), $q^{*2} = u^{*2} + w^{*2}$; like $F^*(\psi^*)$, $G^*(\psi^*)$ is implied in the specification of $q^*$ and $v^*$ at $r^* = r_1^*$, and $G^*(\psi^*) = \text{const.}$ is a case of particular interest.

The conservation of momentum in the direction normal to a surface $\psi^* = \text{const.}$ is implied by (cf. (25)).

$$\frac{\partial}{\partial n^*}\left(\frac{p^*}{\rho_d^*}\right) = \frac{v^{*2}\sin\theta}{r^*} - q^{*2}\frac{\partial\theta}{\partial s^*} \quad . \tag{54}$$

This equation must be rewritten for the coordinate system mentioned earlier. It is noted that

$$\frac{\partial p^*}{\partial n^*} = \frac{\partial\psi^*}{\partial n^*}\frac{\partial p^*}{\partial\psi^*} = r^*q^*\frac{\partial p^*}{\partial\psi^*} \quad , \tag{55}$$

and also that

$$\frac{\partial\theta}{\partial s^*} = \frac{1}{(\partial s^*/\partial\theta)} = -\frac{\cos\theta}{(\partial r^*/\partial\theta)} \quad . \tag{56}$$

Thus,

$$\frac{\partial}{\partial\psi^*}\left(\frac{p^*}{\rho_d^*}\right) = \frac{1}{r^*q^*}\left(\frac{v^{*2}\sin\theta}{r^*} + \frac{q^{*2}\cos\theta}{(\partial r^*/\partial\theta)}\right) \quad . \tag{57}$$

In (57), and subsequent equations, it is implied that $\partial(\ )/\partial\psi^*$ is taken with $\theta$ held fixed, and vice versa.

Finally, note is taken of the geometric identity

$$\left(\frac{\partial r^*}{\partial n^*}\right)_{\theta^* \text{ fixed}} = \sin\theta, \tag{58}$$

so that

$$\frac{\partial r^*}{\partial \psi^*} = \frac{\sin\theta}{r^* q^*} \ . \tag{59}$$

Equations (52), (53), (57), and (59) constitute a set of four equations from which the four unknowns $v^*$, $q^*$, $p^*$, and $r^*$ can be calculated, where each unknown is a function of $\psi^*$ and $\theta$.

The appropriate initial conditions are

$$p^* = p_1^* \ , \ r^* = r_1^* \ , \ F^*(\psi^*) \text{ given}, \ G^*(\psi^*) \text{ given on } \theta = \theta_o = 0 \ ,$$
$$0 \leq \psi^* \leq \psi^*_{max} \ . \tag{60}$$

A particularly interesting case is $F^* = (\text{const.})\ \psi^*$, $G^* = (\text{const.})\ \psi^*_{max}$, with $\psi^*_{max}$ calculable.

The boundary conditions are $\left[G^*(\psi^*_{max}) = V^{*2}/2\right]$:

$$p^*(\psi = 0, \theta\ ) = p_1^* \ , \tag{61}$$

$$p^*(\psi^*_{max},\theta) - p_1^* = -\frac{\rho_d^*}{2}\left[v^{*2}(\psi^*_{max},\theta) - V^{*2}\right] = -\frac{\rho_d^* \Gamma^{*2}}{2}\left[\frac{1}{r^{*2}(\psi^*_{max},\theta)} - \frac{1}{r_1^{*2}}\right], \tag{62}$$

where $\Gamma^* \equiv r_1^* V^*$, with $r_1^*, V^*$ (and hence $p_1^*$) given.

The following nondimensionalization is adopted:

$$V = v^*/V^*,\ Q = q^*/V^*,\ \chi = r^*/r_1^*,\ \zeta = z^*/r_1^*,\ P = (p^* - p_1^*)/\rho_d^* V^{*2}, \quad (63)$$

$$F = F^*/\Gamma^{*2},\ \psi = \psi^*/r_1^*\Gamma^*,\ G = G^*/V^{*2}. \quad (64)$$

Then, (57), (59), (52), and (53) become, respectively,

$$P_\psi = \frac{V^2 \sin\theta}{Q\chi^2} + \frac{Q\cos\theta}{\chi\chi_\theta}, \quad (65)$$

$$\chi_\psi = \frac{\sin\theta}{\chi Q}, \quad (66)$$

$$V^2 = \frac{F(\psi)}{2}, \quad (67)$$

$$\frac{Q^2}{2} + \frac{V^2}{2} + P = \frac{G(\psi)}{2} \quad (68)$$

At $r^* = r_1^*$, the thickness of the layer is denoted $h^*$. Under the nondimensionalization, (50) becomes, at $\chi = 1$,

$$\frac{\partial\psi}{\partial\zeta} = -u = \left[G(\psi) - F(\psi)\right]^{1/2}, \quad (69)$$

from (53), with $q^{*2} = u^{*2}$, $p^* = p_1^*$. Hence, at $\chi = 1$, if $h \equiv h^*/r_1^*$,

$$\zeta = \int_0^{\psi} \frac{d\psi_1}{\left[G(\psi_1) - F(\psi_1)\right]^{1/2}} \Rightarrow h = \int_0^{\psi_{max}} \frac{d\psi_1}{\left[G(\psi_1) - F(\psi_1)\right]^{1/2}}. \quad (70)$$

The case of interest, from results for the surface inflow layer, is $G(\psi) = 1$. Here the special case $F(\psi) = \psi/\psi_{max}$ is considered:

$$h = \int_0^{\psi_{max}} \frac{d\psi_1}{\left[1 - (\psi/\psi_{max})\right]^{1/2}} = \psi_{max} \int_0^1 \frac{ds}{[1 - s]^{1/2}} = 2\psi_{max} \; ; \quad (71)$$

hence,

$$\psi_{max} = \frac{h}{2} \; . \quad (72)$$

In general, for choice of $G(\psi)$, $F(\psi)$, (70) gives $\psi_{max}$ as a function of h. Henceforth, $\psi_{max}$ is taken as known and is denoted by C.

The boundary conditions are, from (61), (62), and (63),

$$P = 0 \text{ on } \psi = 0 \; ; \qquad P = \frac{\chi^2 - 1}{2\chi^2} \text{ on } \psi = C. \quad (73)$$

The initial conditions at $\theta = 0$ are, for $0 \leq \psi \leq C$,

$$P = 0, \; \chi = 1, \; V = \left[F(\psi)\right]^{1/2} \equiv V_0(\psi), \; Q = \left[G(\psi) - F(\psi)\right]^{1/2} \equiv Q_0(\psi) \; . \quad (74)$$

For $0 < \theta << 1$, solution is sought in the form

$$Q(\psi,\theta) = Q_0(\psi) + \theta^{1/2} \tilde{q}(\psi) + \ldots, \quad (75)$$

$$P(\psi,\theta) = \quad + \theta^{1/2} \tilde{p}(\psi) + \ldots, \quad (76)$$

$$V(\psi,\theta) = V_0(\psi) \left[1 - \theta^{1/2} \tilde{r}(\psi) - \ldots \right], \quad (77)$$

$$\chi(\psi,\theta) = 1 \quad + \theta^{1/2} \tilde{r}(\psi) + \ldots, \quad (78)$$

Substitution of (75) - (78) in (65) - (68) gives, since (67) becomes an identity,

$$\tilde{p}' = \frac{2Q_o}{\tilde{r}} ; \tag{79}$$

$$\tilde{r}' = 0 \Rightarrow \tilde{r}(\psi) = \text{const} \equiv m ; \tag{80}$$

$$Q_o \tilde{q} - V_o^2 \tilde{r} + \tilde{p} = 0. \tag{81}$$

Thus,

$$\tilde{p}' = \frac{2}{m} Q_o , \quad \tilde{p} = -Q_o \tilde{q} + V_o^2 m. \tag{82}$$

From the first of (73), $\tilde{p}(\psi = 0) = 0$; from the second of (82), $\tilde{q}(0) = 0$ since $V_o^2(\psi = 0) = F(\psi = 0) = 0$. Differentiation of the second of (82), and substitution from the first of (82), give

$$(Q_o \tilde{q})' = -\frac{2}{m} Q_o + m(V_o^2)' ; \tag{83}$$

$$\tilde{q} = \frac{-\frac{2}{m} \int_o^{\psi} Q_o(\psi_1)\, d\psi_1 + m V_o^2}{Q_o} . \tag{84}$$

But at $\psi = C$, $Q = 0$, so $Q_o(C) = \tilde{q}(C) = 0$. From inspection of (85),

$$m^2 = 2 \int_o^{C} Q_o(\psi_1)\, d\psi_1 , \tag{85}$$

since $V_o(C) = 1$. For $G(\psi)$, $F(\psi)$ of interest, (84) gives $\tilde{q} \to 0$ as $\psi \to C$. The quantities $\tilde{r}$, $\tilde{q}$, $\tilde{p}$ have now been determined, so (75) - (78) may be used to initiate the solution.

It is helpful to introduce

$$Q(\psi,\theta) = \left(1 - \frac{\psi}{C}\right)^{1/2} \phi(\psi,\theta), \tag{86}$$

where $\phi(C,\theta)$ is neither singular nor zero. It is also helpful to introduce the following change of one of the independent variables:

$$X = 1 - [1 - (\psi/C)]^{1/2} \Leftrightarrow \psi = C[1 - (1 - X)^2]. \tag{87}$$

Thus,

$$\frac{\partial}{\partial\psi} = \frac{1}{2C[1 - (\psi/C)]^{1/2}} \frac{\partial}{\partial\psi} = \frac{1}{2C(1 - X)} \frac{\partial}{\partial X}; \tag{88}$$

$$Q(X,\theta) = (1 - X)\,\phi\,(X,\theta). \tag{89}$$

Equations (65) - (68) are transformed as follows:

$$\frac{1}{2C} P_X = \frac{V^2 \sin\theta}{\phi X^2} + \frac{(1 - X)^2\,\phi\cos\theta}{X X_\theta}, \tag{90}$$

$$\frac{1}{2C} X_X = \frac{\sin\theta}{X\phi}, \tag{91}$$

$$V^2 = \frac{F[\psi(X)]}{X^2}, \tag{92}$$

$$\frac{(1 - X)^2\,\phi^2}{2} + \frac{V^2}{2} + P = \frac{G[\psi(X)]}{2}. \tag{93}$$

The initial conditions at $\theta = 0$ are, for $0 \leq X \leq 1$, from (74),

$$P = 0,\ X = 1,\ V = F[\psi(X)]^{1/2} = V_o[\psi(X)],$$

$$\phi = \frac{\left\{G[\psi(X)] - F[\psi(X)]\right\}^{1/2}}{1 - X} = \phi_o(X) . \tag{94}$$

The boundary condition on $X = 0$ is, from (73),

$$P(0,\theta) = 0. \tag{95a}$$

If $G[\psi(X)] = 1$ for $\psi = X = 0$, then since $F[\psi(X)] = 0$ for $\psi = X = 0$, from (93),

$$\phi(0,\theta) = 1. \tag{95b}$$

Hence,

$$\chi(0,\theta)\ \chi_X(0,\theta) = 2C \sin\theta \Rightarrow [\chi(0,\theta)]_X = 4C \sin\theta. \tag{96}$$

The boundary condition on $\psi = C$ is now developed. Differentiation of (68) with respect to $\psi$ gives, with (67),

$$QQ_\psi + \frac{F'(\psi)}{2\chi^2} - \frac{F(\psi)\chi_\psi}{\chi^3} + P_\psi = \frac{G'(\psi)}{2} . \tag{97}$$

From (85),

$$QQ_\psi = -\frac{1}{2C}\,\phi\,[\phi + 2(1 - \tfrac{\psi}{C})\,\phi_\psi] . \tag{98}$$

At $\psi \to C$,

$$-\frac{1}{2C}\phi^2 + \frac{F'(C)}{2\chi^2} - \frac{F(C)\chi_\psi}{\chi^3} + P_\psi = \frac{G'(C)}{2} . \tag{99}$$

But as $\psi \to C$,

$$\frac{F(C)\chi_\psi}{\chi^3} = \frac{F(C)\sin\theta}{\chi^4 Q} = P_\psi , \tag{100}$$

so

$$-\frac{1}{2C}\phi^2(C,\theta) + \frac{F'(C)}{2\chi^2} = \frac{G'(C)}{2} \quad \Rightarrow \tag{101}$$

$$\phi^2(X=1,\theta) = \frac{CF'[\psi(X=1)]}{\chi^2(X=1,\theta)} - CG'[\psi(X=1)] . \tag{102}$$

If $G'[\psi(X=1)] = 0$,

$$\phi^2(X=1,\theta) = \frac{CF'[\psi(X=1)]}{\chi^2(X=1,\theta)} ; \tag{103}$$

$$\chi_X(X=1,\theta) = \frac{2C^{1/2}\sin\theta}{F'[\psi(X=1)]^{1/2}} . \tag{104}$$

The boundary-value problem is now of initial-value, or marching type, a significant simplification over (9), (11), and (14). If the solution for $P(X,\theta)$ $V(X,\theta)$, $\phi(X,\theta)$, and $\chi(X,\theta)$ is known at $\theta = \theta_i$, then upon assignment of $F[\psi(X)]$ and $G[\psi(X)]$, the solution may be found at $\theta = \theta_{i+1} > \theta_i$.

One might proceed via adoption of an explicit finite-difference treatment of (90), by means of a four-point grid element with central spatial differencing and with special provision for enforcement of the boundary conditions (96) and (104) at X = 0,1. One may then obtain $\phi(X,\theta_{i+1})$ from (91) by simple differentiation $V(X,\theta_{i+1})$ from (92) by simple substitution, and $P(X,\theta_{i+1})$ from (93) by simple substitution. The procedure may then be repeated to obtain values for the dependent variables as a function of X at the next increment in the time-like variable $\theta_{i+2}$. Unfortunately the accuracy of this fully finite-differenced procedure proves to be insufficient.

Instead, the method of lines (refs. 51-53) is used, such that only the derivatives with respect to X are finite-differenced; as a result, coupled nonlinear ordinary differential equations, each of the first order, must be integrated forward in $\theta$ from specified initial values. Specifically, (97) is written, by use of (91) and (92), as

$$\frac{d\chi_j(\theta)}{d\theta} - \frac{2C^2\sin^2\theta(1 - X_j)^2}{(\chi_j)^2(\chi_X)_j}\left[(P_X)_j - \frac{(\chi_X)_j}{(\chi_X)^3}\right]^{-1}, \quad j = 1,2,\ldots,N \tag{105}$$

where $\chi_j(\theta) \equiv \chi(X_j,\theta)$, with $X_1 = 0$, $X_N = 1$, and $X_{j+1} > X_j$. The $X_j$ are chosen, along with N, the number of points used to resolve the structure in X for each $\theta$. For the special case $G[\psi(X)] = 1$, from (91)-(93),

$$(P_X)_j = -\frac{(F_X)_j}{(\chi_j)^2} + \frac{(\chi_X)_j}{(\chi_j)^3} + \frac{4C^2\sin^2\theta(1 - X_j)}{(\chi_j)^2\ (\chi_X)_j^{\ 2}} + \frac{4C^2\sin^2\theta(1 - X_j)^2}{(\chi_j)^3\ (\chi_X)_j}\left\{1 + \frac{(\chi_{XX})_j\ \chi_j}{\left[(\chi_X)_j\right]^2}\right\}. \tag{106}$$

Three-part difference formulae linking $\chi_{j+1}(\theta)$, $\chi_j(\theta)$, and $\chi_{j-1}(\theta)$ give $(\chi_X)_j$ and $(\chi_{XX})_j$, and thereby couple the differential equations for $[d\chi_j(\theta)/d\theta]$, j = 1, 2, ..., N. From knowledge of $\chi_j(\theta)$, one may extract $\phi_j(\theta)$, $V_j(\theta)$, and $P_j(\theta)$ by the procedure alluded to in the previous paragraph.

The integration in $\theta$ is initiated at $\theta_1$, where $0 < \theta_1 << \pi/2$; the series expansion gives $\chi_j(\theta_1)$. The boundary conditions at $X_1$ and $X_N$ are enforced in the expressions adopted for $(\chi_X)_1$, $(\chi_{XX})_1$, $(\chi_X)_N$, and $(\chi_{XX})_N$ (ref. 53).

Here the simplest conceivable procedure is adopted as a first trial. The parameter N = 3; in particular,

$$X_1 = 0, \quad X_2 = 1 - \frac{2^{1/2}}{2}, \quad X_3 = 1 \tag{107}$$

for equal mass flux about $X_2$ for the special case $F[\psi(X)] = \psi/C \Rightarrow X(2 - X)$. Thus,

$$(\chi_X)_2 = \frac{(\chi_3 - \chi_2)(X_2 - X_1)^2 + (\chi_2 - \chi_1)(X_3 - X_2)^2}{(X_2 - X_1)(X_3 - X_2)(X_3 - X_1)}; \tag{108}$$

$$(\chi_{XX})_2 = \frac{2\left[(\chi_3 - \chi_2)(X_2 - X_1) - (\chi_2 - \chi_1)(X_3 - X_1)\right]}{(X_2 - X_1)(X_3 - X_2)(X_3 - X_1)} \tag{109}$$

Also, simple two-point differencing is used to express the boundary conditions in terms of $\chi_2(\theta)$:

$$[\chi^2(0,\theta)]_X = 4C \sin\theta \Rightarrow \chi_1(\theta) = \left\{[\chi_2(\theta)]^2 - 4C(X_2 - X_1)\sin\theta\right\}^{1/2}; \tag{110}$$

$$[\chi(1,\theta)]_X = 2C \sin\theta \Rightarrow \chi_3(\theta) = \chi_2(\theta) + 2C(X_3 - X_2)\sin\theta . \tag{111}$$

The entire problem then degenerates to numerical integration of one nonlinear ordinary differential equation for $\chi_2(\theta)$ from $\theta = \theta_1$ to $\theta = (\pi/2)$.

A particular case of interest, as previously noted below (60), is

$$G[\psi(X)] = 1 ; \tag{112}$$

$$F[\psi(X)] = \frac{\psi}{C} \equiv X(2 - X) \Rightarrow F'[\psi(X)] = C^{-1} . \tag{113}$$

It follows that, from (74),

$$Q_o\left(\frac{\psi}{C}\right) = \left(1 - \frac{\psi}{C}\right)^{1/2} \equiv (1 - X); \tag{114}$$

from (85),

$$m = \pm C^{1/2} . \tag{115}$$

From (75), (84), (86), (112), (113), and (114), for small $\theta$,

$$Q[(\psi/C),\theta] = [1 - (\psi/C)]^{1/2} \phi[(\psi/C),\theta] \doteq [1 - (\psi/C)]^{1/2}$$

$$+ \theta^{1/2}\left\{\frac{(\psi/C)}{[1 - (\psi/C)]^{1/2}}\left[m - \frac{2C}{m}\left[1 - \frac{(\psi/C)}{2}\right]\right]\right\}, \tag{116}$$

where

$$\phi[(\psi/C) \to 1,\theta] \to 1 + \theta^{1/2}(-m) . \tag{117}$$

From (76), (82), (112), (113), and (114), for small $\theta$,

$$P[(\psi/C),\theta] \doteq \theta^{1/2}\left\{\left(\frac{2C}{m}\right)\left(\frac{\psi}{C}\right)\left[1 - \frac{(\psi/C)}{2}\right]\right\} . \tag{118}$$

The results of this paragraph may be expressed in terms of X to furnish initial conditions at small but finite $\theta$, with which to commence the numerical integration.

Integration proceeds from $\theta \doteq 0$ to $\theta = (\pi/2)$, where $\chi(0,\theta)$ achieves its minimum value; the solution may be continued by reflection from $\theta = (\pi/2)$ to $\theta = \pi$: e.g.,

$$\chi[X, (\pi/2) - \sigma] = \chi[X, (\pi/2) + \sigma] \qquad (119)$$

where $0 \leq \sigma \leq (\pi/2)$. The solution for $\theta = 0$ to $\theta = (\pi/2)$ is initiated by adopting the negative root in (115), such that $\chi$ decreases with increasing $\theta$, for fixed value of X. Solution for this half of the total "cycle" pertains to the inward excursion of the separated surface inflow layer.

The solution is completed by letting $\theta = \pi - \bar{\sigma}$, $0 \leq \bar{\sigma} \leq (\pi/2)$, in the boundary-value problem posed by (90) - (96), (112) - (113). The dependent variable $\chi$ achieves its maximum value at $X = 1$, $\bar{\sigma} = (\pi/2)$; the solution may be reflected about $\bar{\sigma} = (\pi/2)$, to complete the solution for the "turnaround cycle." Formally, if one identifies $\bar{\sigma}$ with $\theta$, the solution for the outward excursion of the turnaround (discussed in this paragraph) may be obtained from the identical formulation that yields the solution for the inward excursion of the turnaround (discussed in the previous paragraph); the only difference is that one adopts the positive root in (115) in the initializing solution when one seeks results for the outward excursion.

Results obtained by the method of lines to the marching-type boundary-value problem for the turnaround region with structure are given, for swirl profile linear in the normalized streamfunction, and for total head invariant with the normalized streamfunction, in Figs. 12-15. A key result is the very modest overshoot ($\sim$ 10%) of the swirl during inward excursion

of the separated inflow layer. Although the solution warrants considerable refinement, the locus of the low-level "eye wall" is now delineated. Formulation to extend the solution for the "eye wall" properties, in a tractable manner, to the midtroposphere and upper troposphere is now the next logical challenge before modelers of severe tornado structure.

## CONCLUDING REMARKS

Over about the past decade, the authors have used relatively simple analytic methods to study quantitatively a quasisteady, axisymmetric model of a mature severe tornado, taken as a vertical closed system. The procedure has been to adopt locally appropriate simplification to obtain results for subdomains of the vortex; when the results have been obtained, a composite solution should be synthesized from the results for the separate subdomains by requiring suitable continuity of dependent variable and of fluxes at interfaces between subdomains. The methodology was the first, or among the very first, to yield the following results on tornadoes, some of which are now widely accepted.

1. The peak swirl speed in a tornado, relative to the axis of rotation, never much exceeds 110 m/s; the length of the funnel cloud may be used to infer, both readily and quickly, the peak swirl, probably as accurately as more tedious techniques.

2. The pressure reduction from ambient necessary to sustain such a large peak swirl speed may be achieved only if the vortex has two-cell structure, i.e., if the vortex has a central dry nonrotating "eye" of compressionally heated, descending air, situated within an annulus ("eye wall") of swirling air rising on a near-moist-adiabatic locus of thermodynamic states.

3. The mature severe tornado consists, then, of a four-part structure: a potential vortex with the "throughput" supply of warm moist air, in a cyclostrophic balance; a near-ground inflow layer, in which friction dissipates angular momentum, and into which fluid sinks at a slow rate from above; a turnaround, "eyewall," and outflow layer, in which the swirling low-level influx separates from the ground, rises through the vertical extent of the troposphere, and moves radially away from the axis of rotation in the upper troposphere; and the warm "eye," with modestly recirculating flow.

4. The surface inflow layer under the high-speed portion of the vortex consists of a two-part structure: a very thin sublayer, immediately contiguous to the ground, in which frictional effects are significant, and a much thicker region in which an inviscid description suffices. Under a favorable pressure gradient, the thin viscous sublayer becomes thinner as the layer moves inward toward separation into an updraft annulus, while the inviscid portion grows in thickness but modestly with decreasing radial position. In the inviscid portion, the squares of radial and azimuthal velocity components sum to the square of the local potential-vortex speed, at fixed radial position; hence, the large swirl component becomes a large influx component as the ground is approached at fixed radial position, until friction enters very close to the ground to enforce the no-slip boundary condition and to bring the velocity to zero at the ground.

5. The turnaround region, in which the separating surface inflow layer becomes a swirling updraft, is described adequately as an inviscid layer, such that turbulent diffusion is not a central contributor to the dynamic balance (except in a very thin sublayer immediately contiguous to the "eye"). The amount of "overshoot," i.e., the amount by which the swirl in the "corner" flow exceeds the peak value achieved in the potential vortex, is modest.

The next challenge facing such a modeling approach for application to the problem of identifying the occurrence of a mature severe tornado, is restoration of hydrostatic effects, such that the turnaround solution initiated here is continued into the midtroposphere and upper troposphere. Only by so extending the present line of research can properties of the "eye"/"eye wall" interface be delineated. This interface, the unique characteristic of the severe tornado, furnishes the one observable potentially accessible to a passively instrumented, geosynchronous meteorological satellite with mesoscale resolution, for the purpose of detection of the exceptionally dangerous whirlwind. Detection of two-cell structure in a vortex system is far more significant than detection of a Rankine-vortex-type, one-cell structure of a mesocyclone; existence of a mesocyclone by no means necessarily implies the onset of a severe tornado event, but evolution to two-cell structure within a mesocyclone is very highly suggestive of a severe tornado event.

These statements perhaps have implications for the most profitable direction for tornado research aimed at anticipation of the onset of a severe tornado, as opposed to early detection of an already developed, intense whirlwind. Specifically, rather than apply linear stability theory to a two-cell vortex model in order to establish propensity to multiple-vortex (i.e., satellite-vortex) structure, one might better examine the conditions under which transition of a one-cell structure to a two-cell structure is preferred in the swirling system. Indeed, this particular stability problem seems to have been neglected, relative to either the multiple-vortex problem just mentioned, or the oft-examined question of initial organization of a weak depression that ultimately evolves to a mesocyclone.

In view of (1) the insight and convenience derived from explicit and largely closed-form results, (2) the absence of detailed field measurements, and (3) the uncertainties of modeling turbulent diffusion in rapidly swirling atmospheric vortex, the authors believe that such simplified subdivisional modeling of the tornado continues to be the most productive path to delineating whirlwind properties and structure.

TRW Systems and Energy
Redondo Beach, California 90278
31 October 1978

## REFERENCES


1. Dergarabedian, P.; and Fendell, F.: Analytic Studies of Local-Severe-Storm Observables by Satellites. NASA Contractor Report CR-2830, 1977.

2. Lemon, L. R.; Donaldson, Jr., R. J.; Burgess, D. W.; and Brown, R. A.: Doppler Radar Application to Severe Thunderstorm Study and Potential Real-Time Warning. Bull. Amer. Meteorol. Soc., vol. 58, 1977, pp. 1187-1193.

3. Fendell, F. E.: Tropical Cyclones. Advances in Geophysics, vol. 17, H. E. Landsberg and J. Van Meighem, eds., Academic, 1974, pp. 1-100.

4. Dergarabedian, P.; and Fendell, F.: One- and Two-Cell Structure in Tornadoes. Proceedings of the Symposium on Tornadoes: Assessment of Knowledge and Implications for Man, R. E. Peterson, ed., c. 1977, pp. 501-521. (Available from the Institute for Disaster Research, Texas Tech. Univ., Lubbock, Texas).

5. Gray, W. M.: Hypothesized Importance of Vertical Wind Shear in Tornado Genesis. Preprints of Papers Presented at the Sixth Conference on Severe Local Storms, 1969, pp. 230-237. (Available from the American Meteorological Society, Boston, Mass.)

6. Gray, W. M.: Research Methodology, Observations, and Ideas on Tornado Genesis. Preprints of Papers Presented at the Seventh Conference on Severe Local Storms, 1971, pp. 292-298. (Available from the American Meteorological Society, Boston, Mass.)

7. Lilly, D. K.: Tornado Dynamics. Research Ms. 69-117, National Center for Atmospheric Research, Boulder, Colorado, 1969.

8. Dergarabedian, P.; and Fendell, F.: On Estimation of Maximum Wind Speeds in Tornadoes and Hurricanes. J. Astronaut. Sci., vol. 17, 1970, pp. 218-236.

9. Dergarabedian, P. and Fendell, F.: One- and Two-Cell Tornado Structure and Funnel-Cloud Shape. J. Astronaut. Sci., vol. 21, 1973, pp. 26-31.

10. Gutman, L. N.: Theoretical Model of a Waterspout. Bull. Acad. Sci., Geophys. Ser. 1957, no. 1, 1957, pp. 87-103.

11. Sullivan, R. D.: A Two-Cell Vortex Solution of the Navier Stokes Equation. J. Aerospace Sci., vol. 26, 1959, pp. 767-768.

12. Kuo, H. L: On the Dynamics of Convective Vortices. J. Atmospheric Sci., vol. 23, 1966, pp. 25-42.

13. Kuo, H. L.: Note on the Similarity Solutions of the Vortex Equations in an Unstably Stratified Atmosphere. J. Atmospheric Sci., vol. 24, 1967, pp. 596-597.

14. Bellamy-Knights, W. M.: An Unsteady Two-Cell Vortex Solution of the Navier-Stokes Equations. J. Fluid Mech., vol. 41, 1970, pp. 673-687.

15. Kendall, W. M.: Unsteady Two-Cell Similarity Solution to a Convective Atmospheric Vortex Model. Tellus, vol. 30, 1978, pp. 376-382.

16. Darkow, G. L.: Periodic Tornado Production by Long-Lived Parent Thunderstorms. Preprints of Papers Presented at the Seventh Conference on Severe Local Storms, 1971, pp. 214-217. (Available from the American Meteorological Society, Boston, Mass.)

17. Darkow, G. L.: Tornado Detection, Tracking and Warning. Proceedings of the Symposium on Tornadoes: Assessment of Knowledge and Implications for Man, R. E. Peterson, ed., c. 1977, pp. 243-247. (Available from Institute for Disaster Research, Texas Tech. Univ. Lubbock, Tex.)

18. Brandes, E. A.: Mesocyclone Evolution and Tornadogenesis: Some Observations. Mon. Weather Rev., vol. 106, 1978, pp. 995-1011.

19. Fujita, T. T.; Forbes, G. S.; and Umenhofer, T. A.: Close-up View of 20 March 1976 Tornadoes: Sinking Cloud Tops to Suction Vortices. Weatherwise, vol. 29, 1975, pp. 116-131.

20. Anonymous: Flight over a Tornado-Bearing Thunderstorm. Bull. Amer. Meteorol. Soc., vol. 58, 1977, pp. 608-609.

21. Davis-Jones, R.; and Kessler, E.: Tornadoes. Weather and Climate Modification, W. N. Hess, ed., John Wiley, 1974, pp. 552-595.

22. Emmons, H. W.; and Ying, S.-J.: The Fire Whirl. Eleventh Symposium (International) on Combustion, Combustion Institute, 1967, pp. 475-486.

23. Greenspan, H. P.: The Theory of Rotating Fluids. Cambridge Univ. Press, 1968.

24. Dergarabedian, P.; and Fendell, F.: Parameters Governing the Generation of Free Vortices. Phys. Fluids, vol. 10, 1967, pp. 2293-2299.

25. Smith, R. K.; and Leslie, L. M.: Tornadogenesis. Quart. J. R. Met. Soc., vol. 104, 1978, pp. 189-199.

26. Lewellen, W. S.: Theoretical Models of the Tornado Vortex. Proceedings of the Symposium on Tornadoes: Assessment of Knowledge and Implications for Man, R. E. Peterson, ed., c. 1977, pp. 107-143. (Available from the Institute for Disaster Research, Texas Tech. Univ., Lubbock, Tex.)

27. Lewellen, W. S.; and Teske, M. E.: Turbulent Transport Model of Low-Level Winds in a Tornado. Preprints Tenth Conference on Severe Local Storms, 1977, pp. 291-298. (Available from the American Meteorological Society, Boston, Mass.)

28. Rodenhuis, D. R.; and Anthes, R. A.: Hurricanes and Tropical Meteorology. Bull. Amer. Meteorol. Soc., vol. 59, 1978, pp. 790-803.

29. Turner, J. S.: The Constraints Imposed on Tornado-Like Vortices by the Top and Bottom Boundary Conditions. J. Fluid Mech., vol. 25, 1966, pp. 377-400.

30. Barcilon, A.: Vortex Decay above a Stationary Boundary. J. Fluid Mech., vol. 27, 1967, pp. 155-175.

31. Deissler, R. G.: Models for Some Aspects of Atmospheric Vortices. J. Atmos. Sci., vol. 34, 1977, pp. 1502-1517.

32. Roshko, A.: Structure of Turbulent Shear Flows: A New Look. AIAA J., vol. 14, 1976, pp. 1349-1357.

33. Peterson, R. E.: In Pursuit of Dust Devils. Weatherwise, vol. 29, 1976, pp. 1349-1357.

34. Fujita, T. T.: History of Suction Vortices. Proceedings of the Symposium on Tornadoes: Assessment of Knowledge and Implications for Man, R. E. Peterson, ed., c. 1977, pp. 78-88. (Available from the Institute for Disaster Research, Texas Tech. Univ., Lubbock, Tex.)

35. Chi, S. W.; Ying, S. J.; and Chang, C. C.: The Ground Turbulent Boundary Layer of a Stationary Tornado-Like Vortex. Tellus, vol. 21, 1969, pp. 693-700.

36. Chi, S. W.; and Glowachi, W. J.: Applicability of Mixing Length Theory to Turbulent Boundary Layers Beneath Intense Vortices. J. Appl. Mech., vol. 41E, 1974, pp. 15-19.

37. Carrier, G. F.: Swirling Flow Boundary Layers. J. Fluid Mech., vol. 49, 1971, pp. 133-144.

38. Burggraf, O. R.; Stewartson, K.; and Belcher, R.: Boundary Layer Induced by a Potential Vortex. Phys. Fluids, vol. 14, 1971, pp. 1821-1833.

39. Carrier, G. F.; and Fendell, F. E.: Analysis of the Near-Ground Wind Field of a Tornado with Steady and Spatially Varying Eddy Viscosity. Wind Field and Trajectory Models for Tornado-Propelled Objects (EPRI Project 308, Rept. NP-748), 1978, pp. A-1 – A-45. (Available from Electric Power Research Institute, Palo Alto, Calif.)

40. Prahlad, T. S.; and Head, M. R.: Numerical Solutions for Boundary Layers Beneath a Potential Vortex. Computers and Fluids, vol. 4, 1976, pp. 157-169.

41. Kuo, H. L.: Axisymmetric Flows in the Boundary Layer of a Maintained Vortex. J. Atmos. Sci., vol. 28, 1971, pp. 20-41.

42. Ying, S. J.; and Chang, C. C.: Exploratory Model Study of Tornado-Like Vortex Dynamics. J. Atmos. Sci., vol. 27, 1970, pp. 3-27.

43. Chi, S. W.: Numerical Modeling of Ground Turbulent Boundary Layers of Intense Atmospheric Vortices. Second U.S. National Conference on Wind Engineering Research, J. E. Cermak, ed., c. 1975, pp. II-4-1-II-4-3. (Available from the Wind Engineering Research Council, J. E. Cermak, chairman, Colorado State University, Fort Collins, Colorado.)

44. Dergarabedian, P.; and Fendell, F. E.: A Method for Rapid Estimation of Maximum Tangential Wind Speed in Tornadoes. Mon. Weather Rev., vol. 99, 1971, pp. 143-145.

45. Hoecker, Jr., W. H.: Wind Speed and Air Flow Patterns in the Dallas Tornado of April 2, 1957. Mon. Weather Rev., vol. 88, 1960, pp. 167-180.

46. Savino, J. M.; and Keshock, E. G.: Experimental Profiles of Velocity Components and Radial Pressure Distributions in a Vortex Contained in a Short Cylindrical Chamber. NASA Technical Note TN D-3072, 1965. (Available from National Aeronautics and Space Administration, Washington, D.C.)

47. Chi, J.: Numerical Analysis of Turbulent End-Wall Boundary Layers of Intense Vortices. J. Fluid Mech., vol. 82, 1977, pp. 209-222.

48. Staats, W. F.; and Turrentine, C. M.: Some Observations and Radar Pictures of the Blackwell and Udall Tornadoes of May 25, 1955. Bull. Amer. Meteorol. Soc., vol. 37, 1956, pp. 495-505.

49. Dinwiddie, F. B.: Waterspout-Tornado Structure and Behavior at Nags Head, N. C., August 12, 1952. Mon. Weather Rev., vol. 87, 1959, pp. 239-250.

50. Davies-Jones, R. P.; Burgess, D. W.; Lemon, L. R.; and Purcell, D.: Interpretation of Surface Marks and Debris Patterns from the 24 May 1973 Union City, Oklahoma Tornado. Mon. Weather Rev., vol. 106, 1978, pp. 12-21.

51. Ames, W. F.: Nonlinear Partial Differential Equations in Engineering. Academic, 1965.

52. Mikhlin, S. G.; and Smolitskiy, K. I.: Approximate Methods for Solution of Differential and Integral Equations. Elsevier, 1967.

53. Ames, W. F.: Numerical Methods for Partial Differential Equations, 2nd. ed. Academic, 1977.

Table 1. Numerical Results for Extrema of the Turnaround, from Integration of the Initial-Value Problem (31)-(33).

| $\alpha$ | $\beta$ | $\alpha/\beta$ | $\bar{x}'(0) \equiv \bar{x}_0'$ | $(\bar{x}^-)_{calc}$ | $(\bar{x}^-)_{\alpha=0}$ | $(\bar{x}^+)_{calc}$ | $(\bar{x}^+)_{\alpha=0}$ |
|---|---|---|---|---|---|---|---|
| 0.1 | 0.1 | 0.0 | 2.0 | 0.791 | 0.789 | 1.264 | 1.266 |
| 0.0 | 0.1 | 0.0 | 5.0 | 0.754 | 0.751 | 1.326 | 1.329 |
| 0.0 | 0.1 | 0.0 | 10.0 | 0.742 | 0.738 | 1.348 | 1.352 |
| 0.0 | 0.1 | 0.1 | 100.0 | 0.732 | 0.727 | 1.366 | 1.372 |
| 0.0 | 0.2 | 0.0 | 2.0 | 0.718 | 0.714 | 1.392 | 1.397 |
| 0.0 | 0.2 | 0.0 | 5.0 | 0.671 | 0.664 | 1.489 | 1.497 |
| 0.0 | 0.2 | 0.0 | 10.0 | 0.656 | 0.647 | 1.524 | 1.533 |
| 0.0 | 0.2 | 0.0 | 100.0 | 0.644 | 0.632 | 1.553 | 1.565 |
| 0.1 | 0.1 | 1.0 | 2.0 | 0.820 | 0.789 | 1.295 | 1.266 |
| 0.1 | 0.1 | 1.0 | 5.0 | 0.777 | 0.751 | 1.348 | 1.329 |
| 0.1 | 0.1 | 1.0 | 10.0 | 0.762 | 0.738 | 1.366 | 1.352 |
| 0.1 | 0.1 | 1.0 | 100.0 | 0.750 | 0.727 | 1.381 | 1.372 |
| 0.1 | 0.2 | 0.5 | 2.0 | 0.748 | 0.714 | 1.422 | 1.397 |
| 0.1 | 0.2 | 0.5 | 5.0 | 0.695 | 0.664 | 1.510 | 1.497 |
| 0.1 | 0.2 | 0.5 | 10.0 | 0.677 | 0.647 | 1.541 | 1.533 |
| 0.1 | 0.2 | 0.5 | 100.0 | 0.663 | 0.632 | 1.567 | 1.566 |
| 0.1 | 0.5 | 2.0 | 2.0 | 0.876 | 0.846 | 1.212 | 1.181 |
| 0.1 | 0.5 | 2.0 | 5.0 | 0.841 | 0.818 | 1.244 | 1.223 |
| 0.1 | 0.5 | 2.0 | 10.0 | 0.828 | 0.808 | 1.254 | 1.237 |
| 0.1 | 0.5 | 2.0 | 100.0 | 0.818 | 0.800 | 1.264 | 1.250 |
| 0.2 | 0.1 | 2.0 | 2.0 | 0.845 | 0.789 | 1.325 | 1.266 |
| 0.2 | 0.1 | 2.0 | 5.0 | 0.796 | 0.751 | 1.369 | 1.329 |
| 0.2 | 0.1 | 2.0 | 10.0 | 0.779 | 0.738 | 1.384 | 1.352 |
| 0.2 | 0.1 | 2.0 | 100.0 | 0.765 | 0.727 | 1.396 | 1.372 |
| 0.2 | 0.2 | 1.0 | 2.0 | 0.774 | 0.714 | 1.452 | 1.397 |
| 0.2 | 0.2 | 1.0 | 5.0 | 0.716 | 0.664 | 1.530 | 1.497 |
| 0.2 | 0.2 | 1.0 | 10.0 | 0.695 | 0.647 | 1.558 | 1.533 |
| 0.2 | 0.2 | 1.0 | 100.0 | 0.678 | 0.632 | 1.581 | 1.566 |
| 0.2 | 0.4 | 0.5 | 2.0 | 0.685 | 0.615 | 1.652 | 1.606 |
| 0.2 | 0.4 | 0.5 | 5.0 | 0.617 | 0.550 | 1.789 | 1.772 |
| 0.2 | 0.4 | 0.5 | 10.0 | 0.594 | 0.528 | 1.838 | 1.832 |
| 0.2 | 0.4 | 0.5 | 100.0 | 0.578 | 0.509 | 1.877 | 1.887 |

Notes: Results for $(\bar{x}^{\pm})_{\alpha=0}$ are from (40). Also, $\bar{x}$ for $\bar{x}_0'$ = 100 are within 2% of values for $\bar{x}_0' \to \infty$, for $\alpha,\beta$ studied.

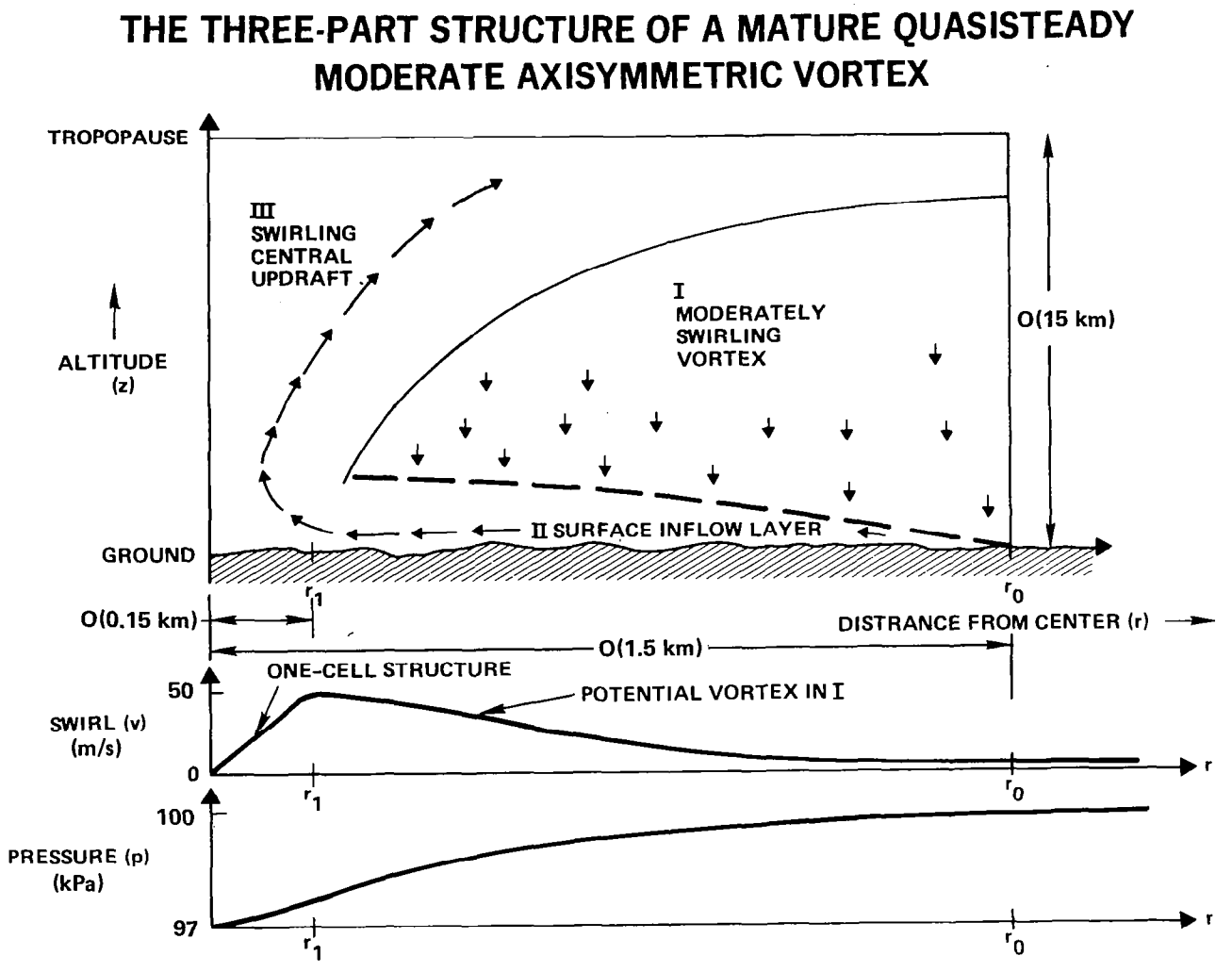


Figure 1. A schematic, not to scale, of a tornado, with 40-m/s peak swirl relative to the axis of symmetry. The radial profile of the swirl, at midtropospheric altitude, is like that of a Rankine vortex. The peak pressure deficit from ambient, at ground, is about 3 kPa. Asterisk superscripts to denote dimensional quantities have been omitted.

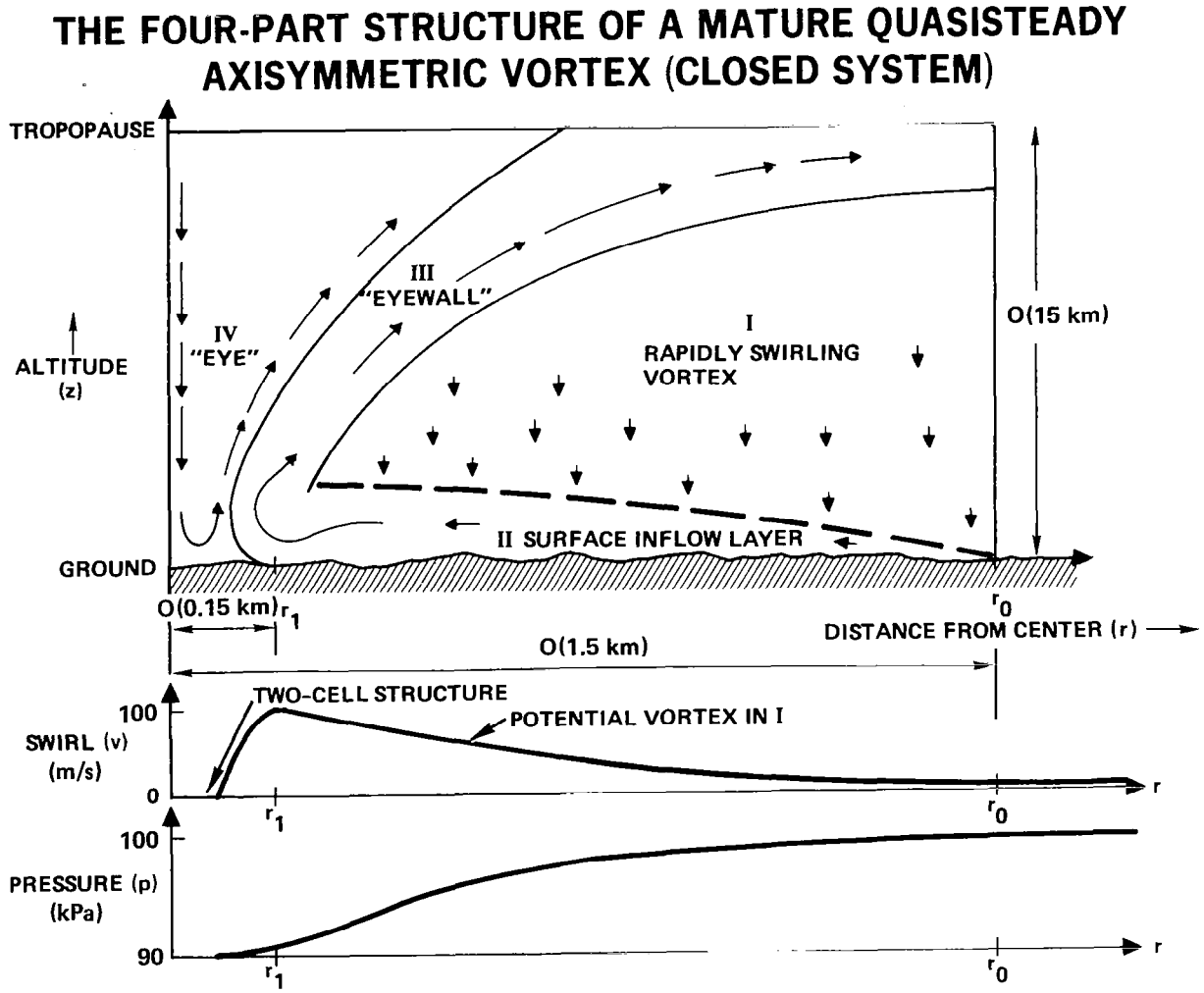


Figure 2. A schematic, not to scale, of the structure of a tornado, with 100-m/s peak swirl relative to the axis of symmetry. The radial profile of the swirl, at midtropospheric altitude, reveals a nonrotating central "eye" joined to a nearly potential vortex. The pressure deficit from ambient, at ground level, may reach about 10 kPa; the outwardly sloped "eye"/"eye wall" interface permits fluid in the potential-vortex portion of the tornado to achieve swirl speeds consistent with this pressure deficit. Asterisk superscripts to denote dimensional quantities have been omitted.

# THE BOUNDARY - VALUE PROBLEM

CONTINUITY $\quad (ru)_r + (rw)_z = 0$

RADIAL MOMENTUM $\quad \dfrac{(rV)^2 - (rv)^2 - (ru)^2}{r^2} = [\nu(ru)_z]_z - u(ru)_r - w(ru)_z$

ANGULAR MOMENTUM $\quad [\nu(rv)_z]_z - u(rv)_r - w(rv)_z = 0$

BOUNDARY CONDITIONS: $\quad z \to \infty$: $v \to \Gamma/r$, $u \to 0$

$z = 0$: $u = v = w = 0$

$r = r_o$: $u = 0$, $v \doteq \Gamma/r_o$

$$\nu = \nu_{mol} + \nu_{eddy}, \quad \nu_{eddy} = \begin{cases} \kappa^2 z^2 (u_z^2 + v_z^2)^{1/2}, & 0 \leq z \leq z_1(r) \\ k_2(\Gamma/r)\delta^*(r), & z_1(r) \leq z \leq \infty \end{cases}$$

$$\delta^*(r) = \int_0^\infty \left(1 - \frac{rv}{\Gamma}\right) dz; \quad k_2(\Gamma/r)\delta^*(r) = \kappa^2 [z_1(r)]^2 \left\{ u_z^2[r, z_1(r)] + v_z^2[r, z_1(r)] \right\}^{1/2}$$

SOLUTION: $ru = -\Gamma\beta(r)g'(\eta)$, $rv = \Gamma f(\eta)$, $w = W(\eta)$

$$\eta = z/s(r), \quad s = r_o[(r_o - r)/(r_o + r)]^{1/2}, \quad \beta^2 = 1 - (r/r_o)^2$$

$g'^2 = 1 - f^2$, $[H(\eta)f']' + gf' = 0$

$f = g = 0$ at $\eta = 0$; $f \to 1$ as $\eta \to \infty$

} MUST PICK $f'(0), \eta_1$; $W(\eta)$ FOLLOWS

Figure 3. The third-order parabolic boundary-value problem for time-averaged description of the turbulent surface inflow layer under a potential vortex over a flat smooth nonrotating boundary. An approximate similarity solution holding over the bulk of the thickness of the layer, under the high-speed portion of the vortex, is developed formally. This solution must be supplemented in a thin sublayer, contiguous to the wall, in which the no-slip condition on the radial inflow is enforced. Asterisk superscripts to denote dimensional quantities have been omitted to simplify notation.

## THE PHYSICS OF THE INFLOW LAYER

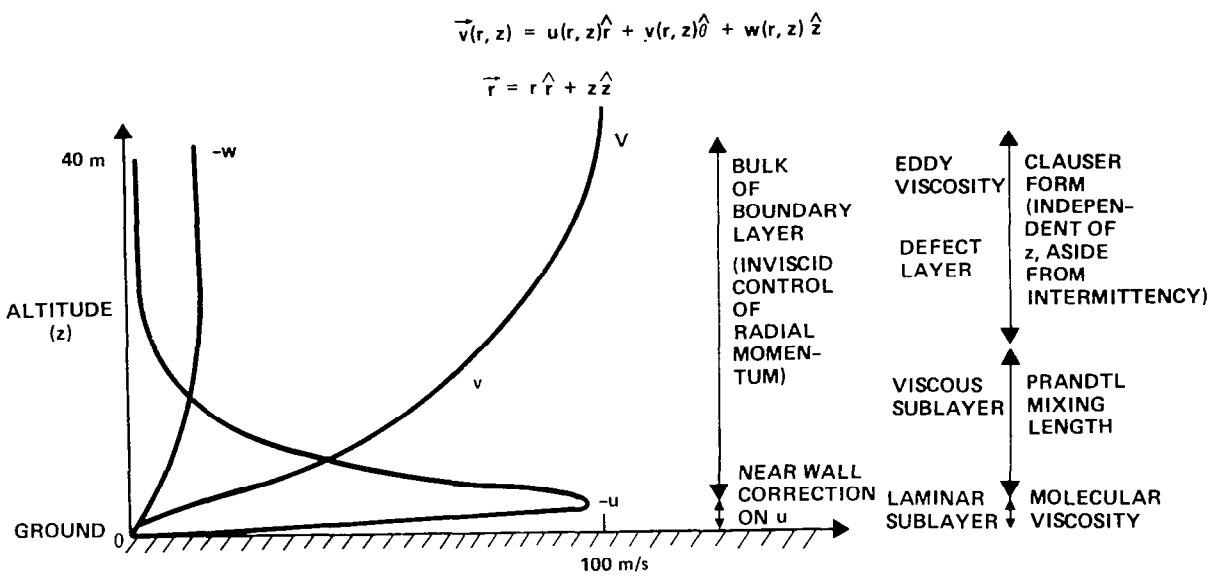


Figure 4. A schematic of the profiles of the velocity components over the entire width of the turbulent boundary layer under the intensely swirling portion of a potential vortex. The radial inflow achieved near the ground is almost as large as the swirl above the inflow layer, at the same radial position. Asterisk superscripts to denote dimensional quantities have been omitted.

# VERBAL INTERPRETATION OF INFLOW LAYER

FAR FROM THE AXIS OF ROTATION ($r_1 \ll r < r_0$)

RADIAL MOMENTUM:

FRICTION, INERTIA, PRESSURE GRADIENT BALANCE

ANGULAR MOMENTUM:

FRICTION, INERTIA BALANCE

CONTINUITY:

SMALL DOWNDRAFT

CLOSER TO THE AXIS OF ROTATION: ($r_1 < r \ll r_0$)

RADIAL MOMENTUM:

INERTIA, PRESSURE GRADIENT BALANCE: $V^2 = u^2 + v^2$

(VERY CLOSE TO WALL, FRICTION ENFORCES NO-SLIP CONDITION)

ANGULAR MOMENTUM:

FRICTION, INERTIA BALANCE (FRICTION SMALL)

CONTINUITY:

SMALL DOWNDRAFT

Figure 5. Further summary of the results of the surface inflow layer analysis. Asterisk superscripts to denote dimensional quantities have been omitted.

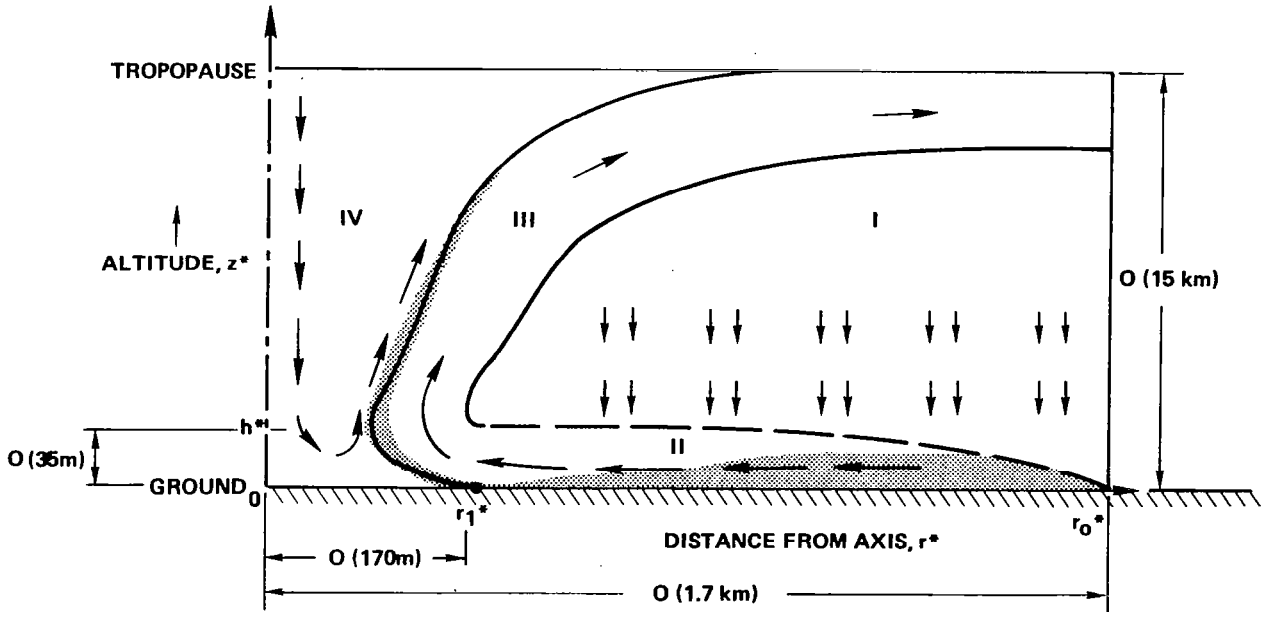


Figure 6. Another schematic diagram, not to scale, of the postulated four-part structure of an idealized mature severe tornado, again taken conveniently as a vertical closed axisymmetric two-cell system extending from ground to tropopause. The arrows indicate the secondary flow (radial and axial velocity compoennt streamlines). The radius of maximum wind (swirl) in I is $r_1^*$; the outer radius of the closed vertical vortex system, $r_0^*$; the maximum depth of the inflow layer, h*. The shaded area suggests where diffusional transfer of momentum is significant.

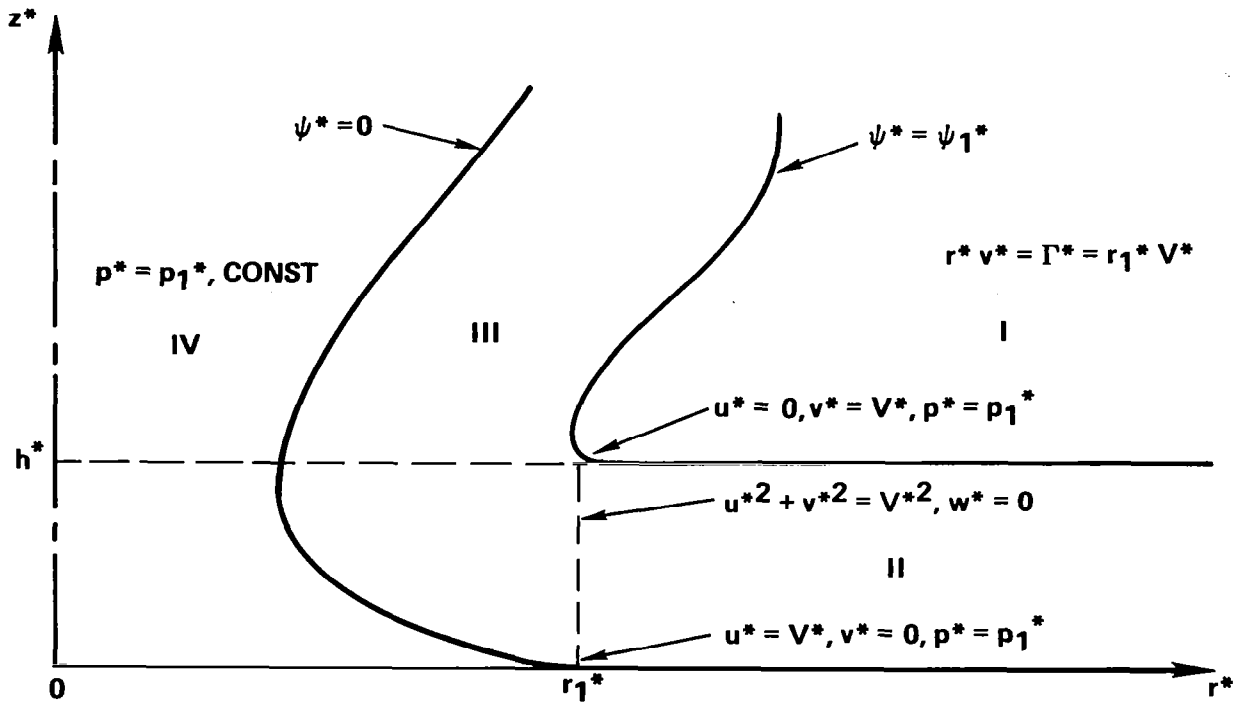


Figure 7. Schematic, not to scale, of an inviscid model of the turnaround region of a severe vertical quasisteady axisymmetric tornado. The "eye", region IV, is isobaric at pressure $p_1^*$, over the vertical extent of interest here, where $p_1^*$ is also the pressure at $r^* = r_1^*$, $z^* = h^*$ (because the pressure is approximately invariant across the surface inflow layer II). The "eye wall", region III, is demarcated by two streamsurfaces, $\psi^*(r^*,z^*)$ = const. (the position of each to be determined), encompassing the mass efflux from region II. It is recalled that a potential vortex holds in region I.

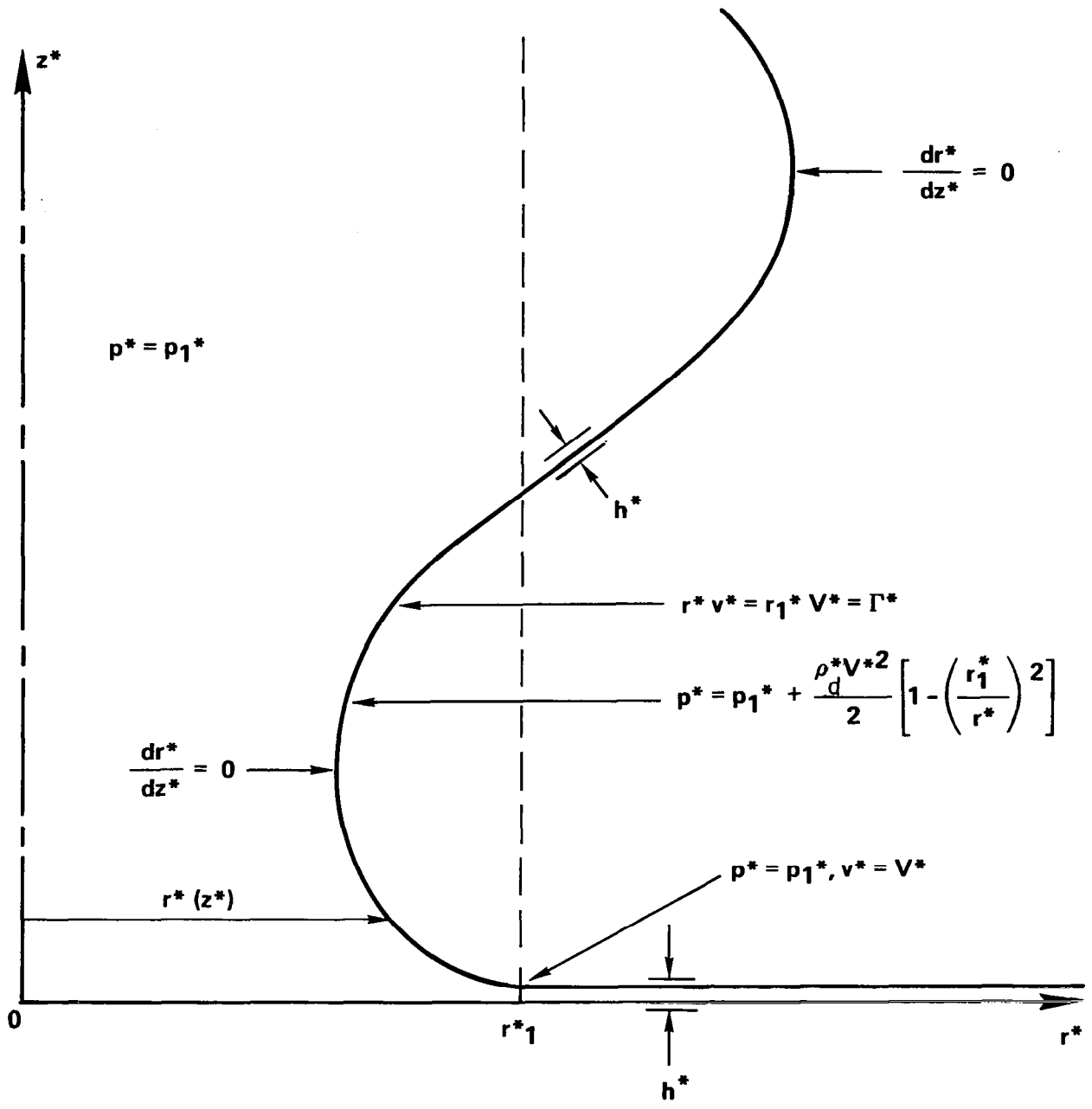


Figure 8. Schematic of the location of an inviscid "eye wall without structure" demarcating the interface between an isobaric non-swirling "eye" at pressure $p_1^*$ and a potential vortex. The sheet representing the "eye wall" has thickness $h^* \to 0$; in the turn-around region, its displacement from the axis, as a function of height above the ground plane, is denoted $r^*(z^*)$.

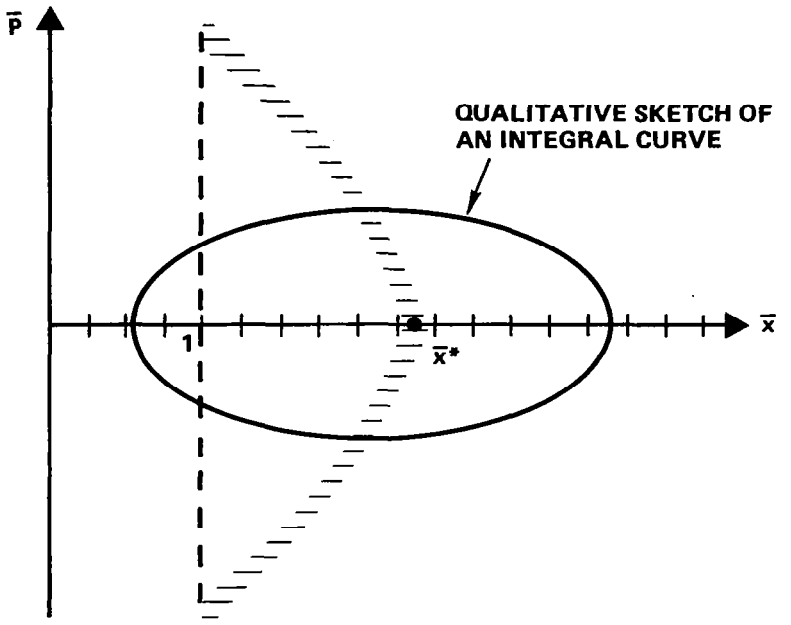


Figure 9. Phase-plane properties of equation (35), where $\bar{P} = (d\bar{x}/d\bar{z})$, with $\bar{x}$ the dependent variable ($\bar{x} > 0$) and $\bar{z}$ the independent variable. Isoclines of zero and infinite slope are noted. At $\bar{x} = 1$, the distance from the axis of symmetry at which the surface inflow layer separates, a finite positive slope is adopted. For $\alpha > 0$, $\bar{x}_* > 1$; for $\alpha = 0$, $\bar{x}_* = 1$. The sketched trajectory (solution curve) is a limit cycle (closed curve indicative of periodic behavior). The periodicity is not of physical interest.

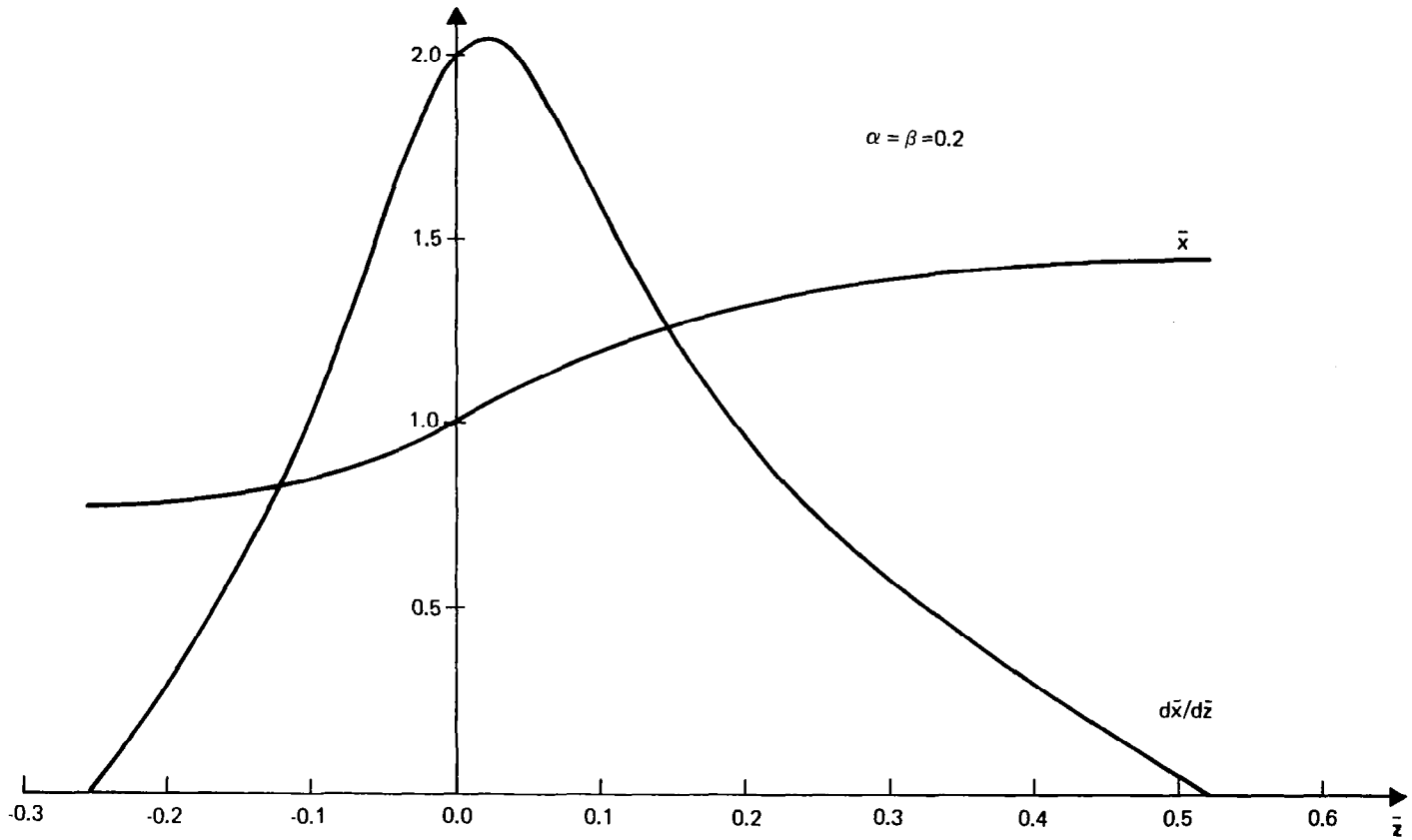


Figure 10. The solution to the boundary-value problem posed by equations (32), (33), and (35), for $\bar{x}_0' = 2$; the solution may be completed by symmetry considerations to constitute a full cycle.

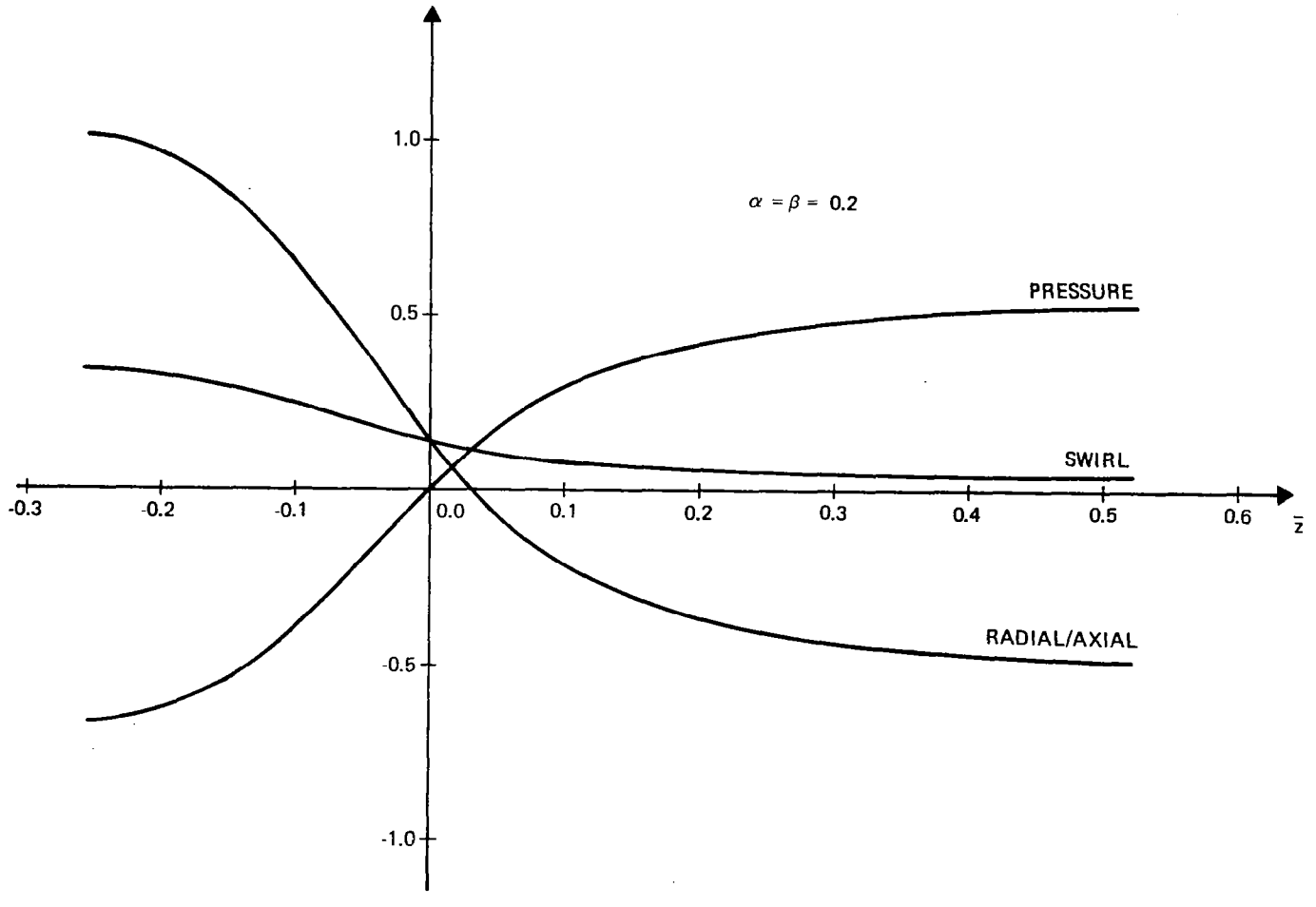


Figure 11. The solution to the boundary-value problem posed by equations (32), (33), and (35), for $\alpha = 0.2$, $\beta = 0.2$, and $\bar{x}_0' = 2$, given in Figure 10, is further discussed. The "pressure" denotes the value of $(1 - \bar{x}^{-2})$; the "swirl" denotes the value of $\alpha\bar{x}^{-3}[1+\bar{x}'^2]^{-1/2}$; the "radial/axial" denotes the value of "swirl" minus "pressure", i.e., the left-hand side of (35).

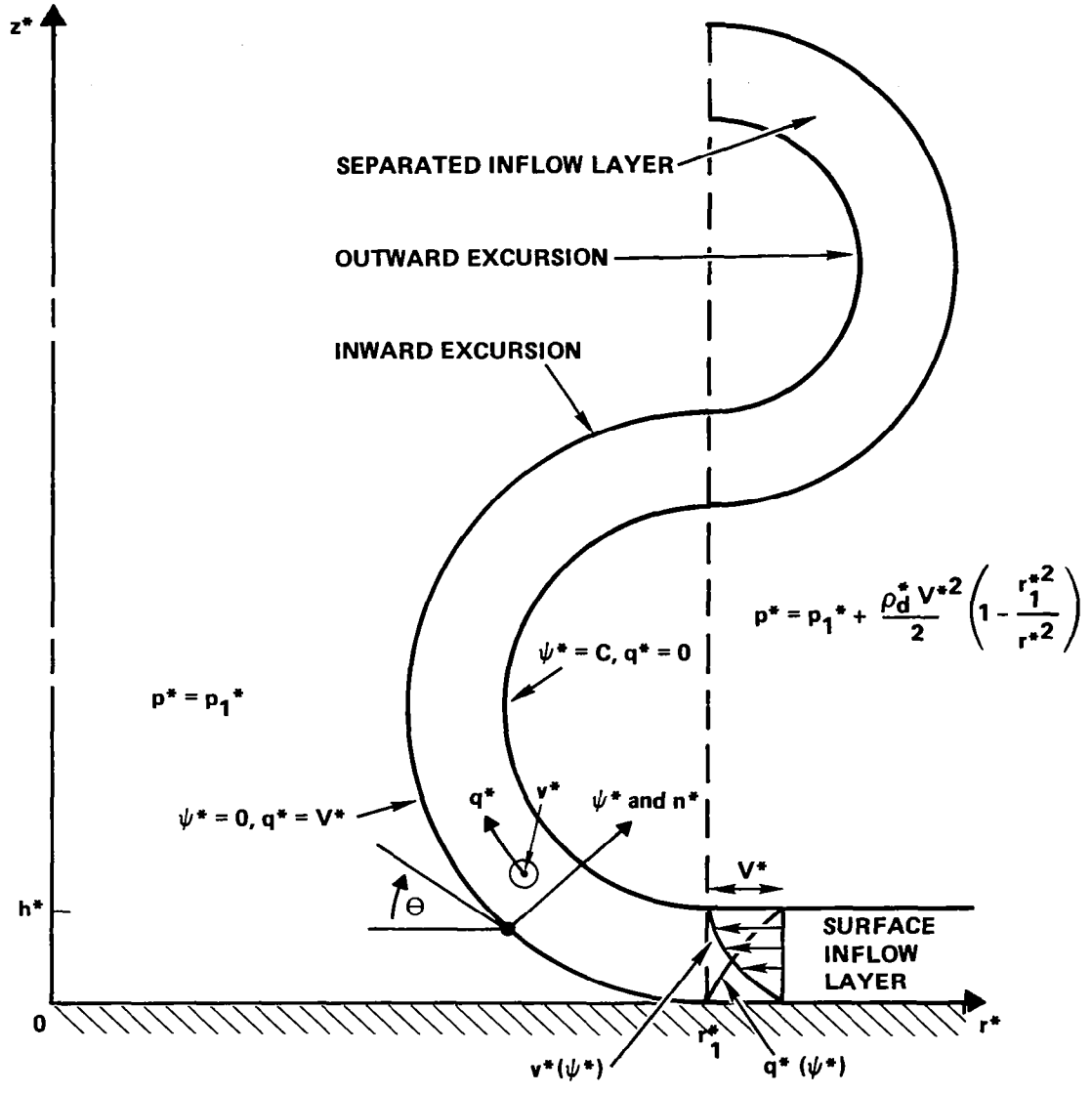


Figure 12. This schematic of the inward, then outward, excursion of the separated inflow layer with structure, indicates the bounding stream surfaces $\psi^* = 0$ and $\psi^* = C$. The in-plane radial-axial flow speed is denoted q*; the swirl about the vertical axis, v*. The inward excursion need be solved for streamfunction-inclination angle $\theta = 0$ to $\theta = (\pi/2)$, since the solution for $\theta = (\pi/2)$ to $\theta = \pi$ may then be obtained by reflection. An analogous statement holds for the outward excursion. The "eye" is isobaric at pressure $p_1^*$, but the potential-vortex pressure varies with radial position r* as noted.

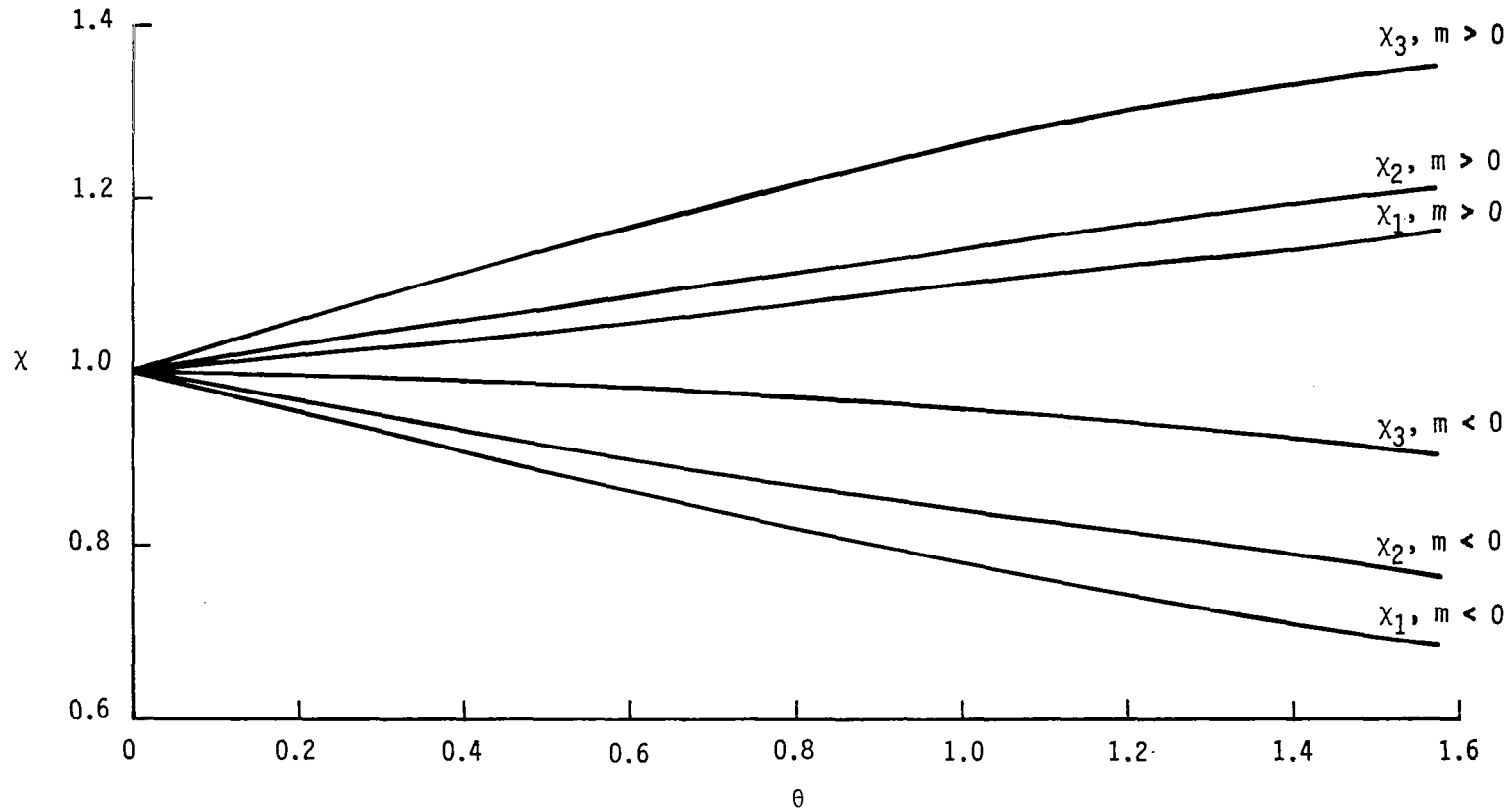


Figure 13. Solution to the boundary-value problem posed by equations (78), (80), (105), (107), (112), and (115), for C = 0.1, as obtained by the method of lines. The notation is that, for example, $\chi_j(\theta) = \chi(\chi_j,\theta)$, where $\chi_j$ is defined in (87), (107). Here the dimensionless radial position $\chi$, defined in (63), is given for the inward excursion ($m < 0$) for $\theta = 0$ to $\theta = (\pi/2)$, and for the outward excursion ($m > 0$) for $(\pi - \theta)$, for $\theta = 0$ to $\theta = (\pi/2)$.

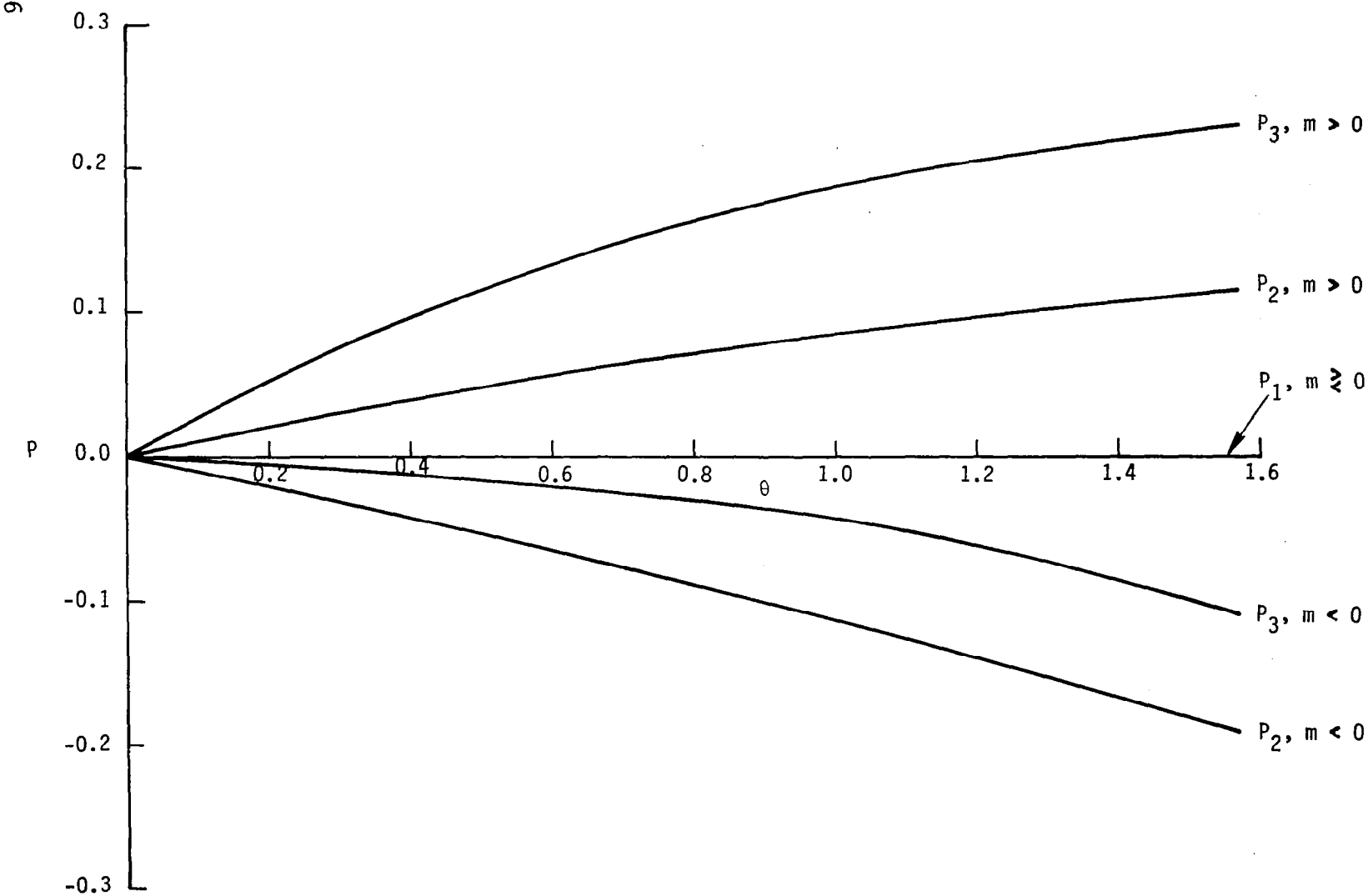


Figure 14. The solution for the dimensionless pressure P, defined in (63), for the problem discussed in Figure 13.

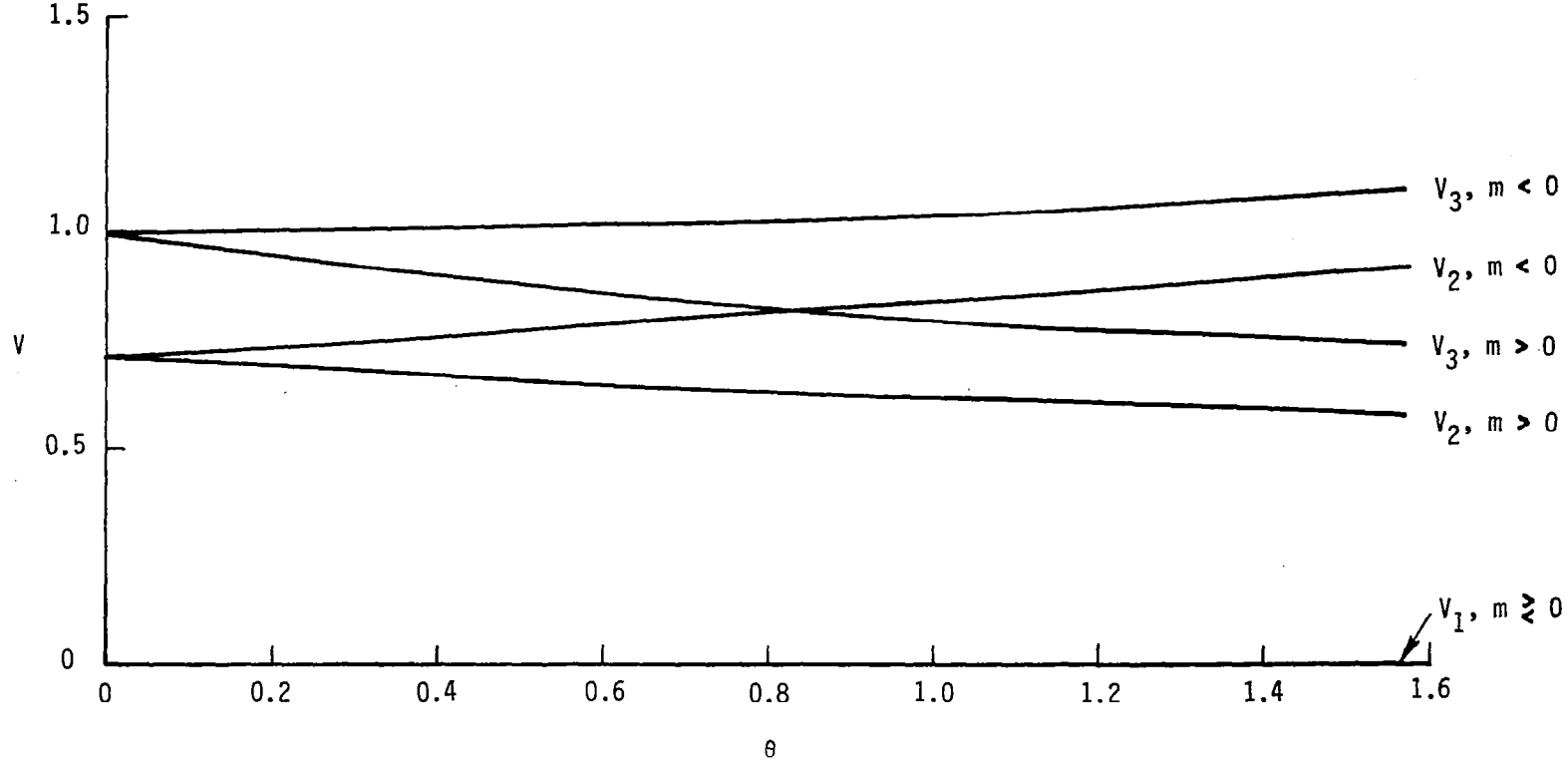


Figure 15. The solution for the dimensionless swirl V, defined in (63), for the problem discussed in Figure 13.

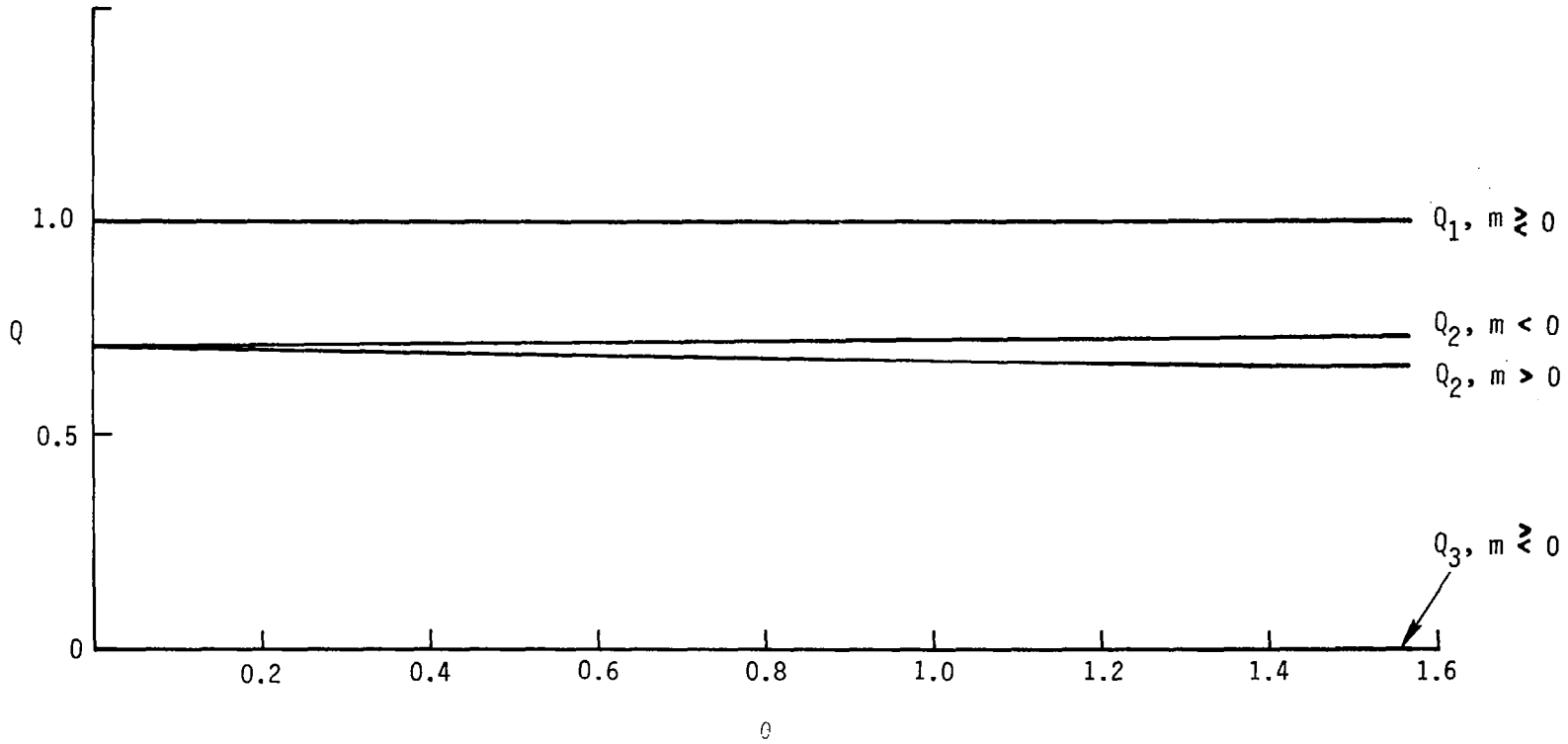


Figure 16. The solution for the dimensionless secondary-flow (in-plane, radial-axial) speed Q, defined in (63), for the problem discussed in Figure 13.

| 1. Report No. | 2. Government Accession No. | 3. Recipient's Catalog No. |
|---|---|---|
| NASA CR-3127 | | |

| 4. Title and Subtitle | 5. Report Date |
|---|---|
| Analytic Studies on Satellite Detection of Severe, Two-Cell Tornadoes | April 1979 |
| | 6. Performing Organization Code |

| 7. Author(s) | 8. Performing Organization Report No. |
|---|---|
| George F. Carrier, Paul Dergarabedian, and Francis E. Fendell | |
| | 10. Work Unit No. |

| 9. Performing Organization Name and Address | 11. Contract or Grant No. |
|---|---|
| TRW Systems and Energy<br>One Space Park<br>Redondo Beach, CA 90278 | NAS1-14578 |
| | 13. Type of Report and Period Covered |
| 12. Sponsoring Agency Name and Address | Contractor Report |
| National Aeronautics and Space Administration<br>Washington, DC 20546 | 14. Sponsoring Agency Code |

15. Supplementary Notes

Langley technical monitor: Robert C. Costen
Final Report

16. Abstract

From funnel-cloud-length interpretation, the severe tornado is characterized by peak swirl speed relative to the axis of rotation of about 90 m/s. Thermohydrodynamic achievement of the pressure deficit from ambient necessary to sustain such swirls requires that a dry, compressionally heated, non-rotating downdraft of initially tropopause-level air lie within an annulus of rapidly swirling, originally low-level air ascending on a near-moist-adiabatic locus of thermodynamic states. The two-cell structure furnishes an observable possibly accessible to a passively instrumented, geosynchronous meteorological satellite with mesoscale resolution, for early detection of a severe tornado. Accordingly, the low-level turnaround region, in which the surface inflow layer separates to become a free ascending layer and for which inviscid modeling suffices, is examined quantitatively. Preliminary results indicate that swirl "overshoot", i.e., swirl speeds in the turnaround region in excess of the maximum achieved in the potential vortex, is modest.

| 17. Key Words (Suggested by Author(s)) | 18. Distribution Statement |
|---|---|
| Rotating thunderstorm<br>Severe local storms<br>Tornado<br>Whirlwind | Unclassified - Unlimited<br>Subject Category 47 |

| 19. Security Classif. (of this report) | 20. Security Classif. (of this page) | 21. No. of Pages | 22. Price* |
|---|---|---|---|
| Unclassified | Unclassified | 70 | $5.25 |

* For sale by the National Technical Information Service, Springfield, Virginia 22161

NASA-Langley, 1979